

# Inertial effects on fibre motion in simple shear flow

By G. SUBRAMANIAN AND DONALD L. KOCH

School of Chemical and Biomolecular Engineering, Cornell University, Ithaca, NY 14853, USA

(Received 27 June 2004 and in revised form 17 January 2005)

The motion of a torque-free slender axisymmetric fibre in simple shear flow is examined theoretically for small but finite  $Re$ , where  $Re$  is the Reynolds number based on the fibre length, and is a measure of the inertial forces in the fluid. In the limit of zero inertia, an axisymmetric particle in simple shear is known to rotate indefinitely in any of an infinite single-parameter family of periodic orbits, originally found by Jeffery (1922) – a degenerate situation wherein the particular choice of orbit is dictated by the initial orientation of the particle. We use a generalization of the well-known reciprocal theorem for Stokes flow to derive the orbit equations, to  $O(Re)$ , for the slender fibre. The structure of the equations bears some resemblance to those previously derived by Leal (1975) for a neutrally buoyant fibre in a viscoelastic (second-order) fluid. It is thereby shown that fluid inertia, for small  $Re$ , leads to a slow  $O(Re)$  drift of the rotating fibre toward the shearing plane, thereby eliminating the aforementioned degeneracy. For Reynolds numbers above a critical value,  $Re_c = (15/4\pi)(\ln \kappa/\beta\kappa) \sin^{-2} \theta$ , the fibre ceases to rotate, however, instead drifting monotonically towards the shearing plane. The limiting stationary orientation in the flow–gradient plane makes an angle  $\phi_f$  with the flow direction, where  $\phi_f = 4\pi Re / (15 \ln \kappa) + \{16\pi Re^2 / (225(\ln \kappa)^2 - 1/(\beta^2 \kappa^2))\}^{1/2}$  is an increasing function of  $Re$ . Here,  $\kappa$  is the fibre aspect ratio,  $\theta$  is the angle made by the fibre with the vorticity axis, and  $\beta$  is an  $O(1)$  coefficient related to the Jeffery period of the rotating fibre.

---

## 1. Introduction

The object of this study is to investigate the effects of fluid inertia on the orientation of non-interacting slender non-Brownian fibres in simple shear flow. Fluid inertia is characterized by the Reynolds number based on the length of the fibre, defined as  $Re = \dot{\gamma} l^2 / \nu$ , where  $l$  is the fibre half-length,  $\dot{\gamma}$  is the shear rate and  $\nu$  is the kinematic viscosity of the suspending fluid. The behaviour of a single fibre in simple shear flow, in the absence of inertia, has been known since the work of Jeffery (1922) on ellipsoids in viscous shear flows. In this limit the velocity disturbance due to the fibre satisfies the quasi-steady Stokes equations; a force-free, torque-free fibre in simple shear then rotates in one of an infinite family of one-parameter closed orbits, the so-called ‘Jeffery’ orbits. The orbits are bounded at one end by a circular orbit in the shearing plane, entailing a tumbling motion, and at the other extreme by a rolling motion of the fibre about the vorticity axis. The particular choice of orbit, however, depends on the initial fibre orientation. Several factors including Brownian motion, hydrodynamic interactions, etc. have therefore been considered by earlier authors (for instance, see Leal & Hinch 1971; Rahnama *et al.* 1993) with the intent of obtaining a unique steady-state orientation distribution. Herein, we consider the presence of inertia in

the suspending fluid as a possible means of eliminating this degeneracy. The present investigation is motivated, in part, by its relevance in the paper and pulp industry, where the orientation distribution of the cellulose fibres in the final paper product is a key determinant of its quality. Since the intermediate processing involves high-speed flows of fibre suspensions, inertial effects may exercise an important influence on the resulting fibre distribution.

We examine the case where  $Re$ , as defined above, is small but finite, the Reynolds number based on the diameter  $d$  of the fibre,  $Re_d = ld\dot{\gamma}/\nu$ , still being negligible. This ensures that the flow in the immediate vicinity of the fibre, i.e. for distances  $r \ll l$ , may still be regarded as a viscous Stokes flow, but that inertia becomes important on scales comparable to or larger than the fibre length. Owing to the high aspect ratio ( $\kappa = 2l/d \gg 1$ ) of the fibre, the techniques of slender-body theory (see Cox 1970; Batchelor 1970 for a detailed description) may be applied to the present problem. This is a singular perturbation method where the velocity disturbance and pressure fields are approximated by quasi-two-dimensional solutions of the Stokes equations in an ‘inner’ region of  $O(d)$  around the fibre axis. These are then matched to the ‘outer’ flow field valid at distances of  $O(l)$ . For our case, the velocity and pressure fields in the outer region must be obtained for small but finite  $Re$  by solving the linearized Navier–Stokes equations, treating the fibre as a line distribution of forces; the linearization becomes possible since the fibre velocity disturbance, at distances of  $O(l)$ , is only  $O(1/\ln \kappa)$  relative to the ambient shear flow. While the above method works in principle, the details of deriving the outer inertial velocity field and subsequent matching of the limiting forms of the flow fields in the inner and outer regions would entail a forbidding amount of algebra. This is, in fact, readily seen in the work of Khayat & Cox (1989), who looked at the effects of inertia in the simpler context of a fibre translating with a fixed orientation in a quiescent fluid.

Therefore, in order to analyse the first effects of fluid inertia on the Jeffery orbits of a single neutrally buoyant torque-free fibre in simple shear flow, we use instead a generalization of the well-known reciprocal theorem (for instance, see Happel & Brenner 1973) for finite  $Re$ . A similar approach has previously been employed for determining the drag on an unsteadily translating spherical particle (see Lovalenti & Brady 1993), and more recently, in the context of the finite- $Re$  rheology of suspensions (see Stone Brady & Lovalenti 2005). It is then shown that the leading-order inertial contribution to the fibre torque is regular, being  $O(Re)$ , and the dominant contribution arises from a region of  $O(l)$  around the fibre. This not only allows neglect of the finite fibre thickness, enabling calculations to be performed in Fourier space, but also helps circumvent the difficulty associated with the non-uniform nature of the leading-order Stokes approximation for the velocity disturbance in an infinite domain (see §3). The latter fact significantly simplifies the analysis. The resulting simplicity is in sharp contrast to the aforementioned matched asymptotic expansion framework, and allows one to focus on the physical mechanisms at work.

There have been several recent numerical investigations of inertial effects in the dynamics of orientable bodies with aspect ratios of order unity, sedimenting under gravity in a quiescent fluid (see Feng, Hu & Joseph 1994), and freely suspended in an ambient shear flow (Aidun, Lu & Ding 1998; Ding & Aidun 2000; Qi & Luo 2003). The only previous work that examines slender-fibre motion analytically at finite Reynolds numbers, however, is that of Khayat & Cox (1989), referred to above, who considered a fibre translating with a fixed orientation; the Reynolds number for this case is  $Re_{sed} = Ul/\nu$ ,  $U$  being the velocity of translation. In the limit  $\kappa \gg 1$ , the outer flow field for this problem is governed by the Oseen equation for a line distribution of

forces, and an analytical determination of the torque becomes possible even for  $O(1)$  values of  $Re_{sed}$ . The authors found the asymmetry of the Oseen solution to lead to a non-zero torque at finite  $Re_{sed}$  for all orientations of the fibre except when it translates with its axis vertical (longitudinal) or horizontal (transverse). The direction of this inertial torque is such that vertical alignment is an unstable fixed point. The fibre thus tends to orient broadside-on for all finite  $Re_{sed}$ , a result intuitively understood by regarding the sedimenting fibre as a line distribution of ‘Oseen-lets’, and keeping in mind the nature of the fore–aft asymmetry of the associated velocity fields for finite  $Re_{sed}$ . In the Appendix we show the applicability of the reciprocal theorem formulation to this problem by rederiving the expression for the finite- $Re_{sed}$  torque. In particular, determining the  $O(Re_{sed})$  torque again requires only knowledge of the corresponding Stokes solution for the velocity disturbance, thereby simplifying the calculation of the first effects of inertia; this is also indicative of the regular nature of the  $O(Re_{sed})$  correction.

We briefly comment on extending the current analysis for perturbative effects of inertia to  $O(1)$  values of  $Re$ . In this regard, it helps to highlight the difference between the problem of a translating (sedimenting) fibre analysed by Khayat & Cox (1989), and that of a neutrally buoyant fibre in simple shear flow. A fibre sedimenting in a quiescent fluid maintains a steady orientation in the Stokes limit. The inertial torque acting to stabilize the transverse orientation is only  $O(1/(\ln \kappa)^2)$  even for  $O(1)$   $Re_{sed}$ , leading to a linear instantaneous relationship between the torque and the induced angular velocity, at leading order, for large  $\kappa$ . This then renders the determination of the torque on a fibre with a fixed orientation, or the angular velocity of a torque-free sedimenting fibre, exactly equivalent. An inertialess fibre in simple shear, for the most part however, behaves as an inextensible material line element, and rotates with the flow. An analytical determination of the fibre angular velocity at  $O(1)$   $Re$  must therefore account for the unsteady contribution arising from its changing history of angular acceleration. This history integral is not known in closed form beyond the simplest cases; indeed, even that for an unsteadily translating sphere at small but finite Reynolds number is extremely involved as evidenced in the work of Lovalenti & Brady (1993). For a slender fibre, the governing Navier–Stokes equations may be linearized to  $O(1/\ln \kappa)$ , but the dependence of the fibre velocity disturbance on its orientation is an added complication. Thus, a rigorous approach must, in essence, solve the full initial value problem. Substantial simplification is possible for a fibre nearly aligned with the flow–vorticity plane, since the fibre angular velocity is vanishingly small for these orientations. This allows for a quasi-steady approximation. The analysis of fibre motion in this limit is the subject of a forthcoming publication. It will be seen later in §3.1 that the aforementioned restriction on fibre orientation is only apparent; the dominant changes in fibre trajectories occur when the inertial corrections to the torque become comparable to the leading-order Jeffery contribution, and this happens precisely for orientations sufficiently close to the flow–vorticity plane.

The paper is organized as follows. In section §2, we describe our approach entailing use of the reciprocal theorem to obtain an expression for the angular velocity of a neutrally buoyant torque-free fibre in simple shear flow at finite  $Re$ . In §3.1 we evaluate the inertial correction to the fibre angular velocity in the limit of small  $Re$ , where knowledge of the leading-order Stokes solution suffices. The governing orbit equations are derived in §3.1.1, and analysed in §3.1.2; the modification to the inertialess fibre trajectories takes the form of an  $O(Re)$  drift. In the limit of infinite aspect ratio, however, the angular velocity of a flow-aligned fibre is zero, and trajectories for both zero and finite  $Re$  approach the flow-aligned orientation for long

times. We therefore include an algebraically small,  $O(\kappa^{-2})$ , term in the equation for the fibre phase, that causes the fibre to rotate across the flow–vorticity plane with an  $O(\kappa^{-2})$  angular velocity; the latter term involves the equivalent aspect ratio of the fibre, defined as  $\kappa_e = \beta\kappa$ ,  $\beta$  being an  $O(1)$  constant related to the Jeffery period of the rotating fibre. This then leads to the degenerate configuration of Jeffery orbits for Stokes flow, and to finite- $Re$  trajectories that spiral out toward the flow–gradient plane. We also compare the predictions of our analysis to previous experimental efforts in this section. Thereafter, in §3.2, we discuss the physical origins for the drift in both fibre orbit and phase, the latter, in particular, allowing for the existence of non-rotating modes for  $Re$  above a critical value. It is argued that for the limits looked at, the motions of a fibre and a dumbbell are similar, and the qualitative effects of inertia remain identical in the two cases. Section 4 is devoted to an analysis of previous related theoretical work. In §5 we consider the motion of a fibre (dumbbell) under the combined effects of sedimentation and shear, again in the limit of weak inertia. The results in this section may be relevant to applications such as the blowing of fibreglass insulation. A typical manufacturing protocol for this involves centrifuging molten glass via the holes on the periphery of a rapidly rotating crown; the radiating filaments are then blasted with a high-velocity gas as they settle to form a mat. The fibre orientation distribution in the final fibreglass mat is thus crucially dependent on the orientation behaviour of the filaments under the effects of both shear and gravity. Finally, §6 presents a summary of the results obtained. In the Appendix, we show that the results of Khayat & Cox (1989) for the inertially induced orientational drift of a sedimenting fibre can be reproduced using the approach adopted in the present study.

## 2. The Generalized Reciprocal theorem and its application to a fibre in simple shear flow

The reciprocal theorem for finite  $Re$  (see Lovalenti & Brady 1993) is given by

$$\int_S \mathbf{n} \cdot \boldsymbol{\sigma}' \cdot \tilde{\mathbf{u}} \, dS + Re \int_V \mathbf{f}' \cdot \tilde{\mathbf{u}} \, dV = \int_S \mathbf{n} \cdot \tilde{\boldsymbol{\sigma}} \cdot \mathbf{u}' \, dS, \quad (2.1)$$

where  $S$  represents all bounding surfaces (including possibly that at infinity,  $S_\infty$ ) and  $\mathbf{n}$  denotes the unit normal directed from  $S$  into the fluid volume  $V$ . The set  $(\mathbf{u}', \boldsymbol{\sigma}', \mathbf{f}')$  corresponds to the given torque-free fibre in simple shear flow, where the position  $\mathbf{r}$ , velocity  $\mathbf{u}'$  and stress tensor  $\boldsymbol{\sigma}'$  have been scaled in the usual manner by  $l$ ,  $\dot{\gamma}l$  and  $\mu\dot{\gamma}$ , respectively. The set  $(\tilde{\mathbf{u}}, \tilde{\boldsymbol{\sigma}})$  represents the solution of an appropriately chosen Stokes flow problem. The primes here are used to denote the disturbance quantities; for instance,  $\mathbf{u}'$  is the disturbance velocity field defined as  $\mathbf{u}' = \mathbf{u} - \boldsymbol{\Gamma} \cdot \mathbf{r}$ ,  $\boldsymbol{\Gamma} = \mathbf{e}_x \mathbf{e}_y$  being the transpose of the velocity gradient tensor in simple shear flow, where  $x$ ,  $y$  and  $z$  correspond to the flow, velocity gradient and vorticity directions, respectively. The inertial terms in the Navier–Stokes equations are denoted by  $\mathbf{f}'$ , given by

$$\mathbf{f}' = \frac{\partial \mathbf{u}'}{\partial t} + \boldsymbol{\Gamma} \cdot \mathbf{u}' + (\boldsymbol{\Gamma} \cdot \mathbf{r}) \cdot \nabla_r \mathbf{u}' + \mathbf{u}' \cdot \nabla_r \mathbf{u}'. \quad (2.2)$$

We choose  $(\tilde{\mathbf{u}}, \tilde{\boldsymbol{\sigma}})$  to correspond to the Stokes flow problem of the same fibre rotating in an otherwise quiescent fluid. For an angular velocity  $\tilde{\boldsymbol{\Omega}}$ ,  $\tilde{\mathbf{u}}$  is then given by

$$\tilde{\mathbf{u}} = \int_{-1}^1 \mathbf{G}_0(\mathbf{r} - s\mathbf{p}) \cdot \tilde{\mathbf{f}}(s\mathbf{p}) \, ds, \quad (2.3)$$

where  $\mathbf{p}$  is a unit vector along the fibre axis,  $\mathbf{G}_0$  is the Oseen tensor given by

$$\mathbf{G}_0(\mathbf{r}) = \frac{1}{8\pi} \left( \frac{\mathbf{I}}{r} + \frac{\mathbf{r}\mathbf{r}}{r^3} \right), \tag{2.4}$$

and  $\tilde{\mathbf{f}}$ , the force per unit length exerted on the fluid by the rotating fibre, is

$$\tilde{\mathbf{f}}(\mathbf{p}s) = \frac{4\pi}{\ln \kappa} (\tilde{\boldsymbol{\Omega}} \wedge \mathbf{p})s, \tag{2.5}$$

where, in the limit of a slender fibre,  $\ln \kappa \gg 1$ . It is to be noted that the above expression for  $\tilde{\mathbf{u}}$ , and the ones below that use (2.3), treat the fibre as a line distribution of forces, the magnitude of the force distribution being correct to  $O(1/\ln \kappa)$ ; higher-order terms of  $O(1/(\ln \kappa)^2)$  are neglected. This approximation remains consistent provided the dominant contributions to the inertial torque do not arise from a region of  $O(d)$  around the fibre. In § 3.1 below, it is shown that the leading-order inertial contribution, in fact, stems from a region surrounding the fibre of order its own length, thereby validating the use of (2.3) and other similar approximations below.

The  $O(1/r^2)$  far-field decay of the velocity disturbances  $\mathbf{u}'$  and  $\tilde{\mathbf{u}}$  now implies that the integrals over  $S_\infty$  may be neglected, and the surface  $S$  in the integrals in (2.1) then reduces to that of the fibre ( $S_f$ ). Using the no-slip boundary conditions for the respective velocity fields on the fibre, the surface integrals reduce to

$$\int_{S_f} \mathbf{n} \cdot \tilde{\boldsymbol{\sigma}} \cdot \mathbf{u}' \, dS = \boldsymbol{\Omega}_p \cdot \tilde{\mathcal{L}} + (\boldsymbol{\Gamma} \cdot \mathbf{p}) \cdot \int_{-1}^1 \tilde{\mathbf{f}}(s\mathbf{p})s \, ds, \tag{2.6}$$

$$\int_{S_f} \mathbf{n} \cdot \boldsymbol{\sigma}' \cdot \tilde{\mathbf{u}} \, dS = \int_{S_f} \mathbf{n} \cdot (\boldsymbol{\sigma} - \boldsymbol{\sigma}^\infty) \cdot \tilde{\mathbf{u}} \, dS \tag{2.7}$$

$$= \tilde{\boldsymbol{\Omega}} \cdot \mathcal{L}'. \tag{2.8}$$

Here  $\boldsymbol{\sigma}^\infty$  is the stress field in the ambient simple shear flow,  $\tilde{\mathcal{L}}$  is the torque on the fibre rotating in a quiescent fluid, and  $\mathcal{L}'$  is the torque arising due to the fibre velocity disturbance in simple shear flow. The surface integrals above have been reduced to line integrals over the axial coordinate  $s$  by integrating over the fibre circumference. The expressions for the velocity and force fields, namely (2.3) and (2.5), are obtained using slender-body theory, and are accurate to  $O(1/\ln \kappa)$ . The inertia of the fibre itself, and the resulting angular acceleration contribute terms that are algebraically small, being only  $O(\kappa^{-2})$  relative to fluid inertial forces, and may again be neglected. Thus,  $\mathcal{L}'$  is zero for a freely rotating fibre, and the resulting angular velocity of the torque-free fibre in simple shear flow,  $\boldsymbol{\Omega}_p$ , is given by

$$(\tilde{\boldsymbol{\Omega}} \wedge \mathbf{p}) \cdot (\boldsymbol{\Omega}_p \wedge \mathbf{p} - \boldsymbol{\Gamma} \cdot \mathbf{p}) = \frac{3 \operatorname{Re}(\ln \kappa)}{8\pi} \int_V \mathbf{f}'(\mathbf{r}) \cdot \tilde{\mathbf{u}}(\mathbf{r}) \, d\mathbf{r}, \tag{2.9}$$

where we have used the expression for  $\tilde{\mathcal{L}}$  obtained from integrating the (antisymmetric) first moment of the force density in (2.5). The volume integral on the right-hand side represents the correction to the fibre rotation rate on account of fluid inertial effects.

### 3. Fibre trajectories for small but finite inertia

#### 3.1. Trajectory analysis for $Re \ll 1$

##### 3.1.1. Derivation of fibre orbit equations

For small but finite  $Re$  the Stokes equations do not provide a uniform approximation for the velocity disturbance field due to a particle in an unbounded domain. The algebraic decay of the leading-order Stokes disturbance field ensures that convection of momentum dominates viscous diffusion beyond an inertial screening length that for simple shear scales as  $lRe^{-1/2}$  – the Saffman length (see Saffman 1965). In the limit  $Re \ll 1$ , it is easily shown that the dominant contribution to the volume integral in (2.9) still comes from a region  $r \sim O(1)$  around the fibre. The contributions from both the inner region ( $r \sim \kappa^{-1}$ ) where the velocity field behaves logarithmically, and the Oseen region ( $r \gg Re^{-1/2}$ ), are asymptotically small, the latter being  $O(Re^{3/2})$  (also see §4). In fact, the contribution from the inner region,  $r \sim \kappa^{-1}$ , scales as  $O(Re\kappa^{-1}(\ln \kappa)^{-1})$ , and therefore may be neglected even for  $O(1) Re$  so long as  $\kappa \gg 1$ . Thus, the  $O(Re)$  contribution to the angular velocity of the fibre is regular, and requires only using the Stokes velocity disturbance due to a torque-free fibre in simple shear flow in the expression (2.2) for  $\mathbf{f}'$ . The Stokes field being only  $O(1/\ln \kappa)$  for a slender fibre, the nonlinear term in (2.2) is  $O(1/\ln \kappa)^2$  and may be neglected. In addition, neglect of the inner region implies that the fibre can now be treated as a line distribution of forces for the purposes of evaluating the volume integral in (2.9). It then becomes more convenient to work in Fourier space, and to this end, the Fourier transform is introduced:

$$\hat{g}(\mathbf{k}) = \int d\mathbf{r} e^{-i2\pi\mathbf{k}\cdot\mathbf{r}} g(\mathbf{r}), \tag{3.1}$$

$$g(\mathbf{r}) = \int d\mathbf{k} e^{i2\pi\mathbf{k}\cdot\mathbf{r}} \hat{g}(\mathbf{k}). \tag{3.2}$$

In transform variables, using the convolution theorem, the volume integral becomes

$$\int \mathbf{f}'(\mathbf{r}) \cdot \hat{\mathbf{u}}(\mathbf{r}) d\mathbf{r} = \int \hat{\mathbf{f}}'(-\mathbf{k}) \cdot \hat{\mathbf{u}}(\mathbf{k}) d\mathbf{k} \tag{3.3}$$

$$= \int \left[ \frac{\partial \hat{\mathbf{u}}'}{\partial t}(-\mathbf{k}) + \boldsymbol{\Gamma} \cdot \hat{\mathbf{u}}'(-\mathbf{k}) - (\boldsymbol{\Gamma}^\dagger \cdot \mathbf{k}) \cdot \nabla_{\mathbf{k}} \hat{\mathbf{u}}'(-\mathbf{k}) \right] \cdot \hat{\mathbf{u}}(\mathbf{k}) d\mathbf{k}. \tag{3.4}$$

We use the following expressions for the Stokes velocity fields  $\hat{\mathbf{u}}'$  and  $\hat{\mathbf{u}}$  in reciprocal space (for instance, see Rahnama *et al.* 1993):

$$\hat{\mathbf{u}}'(\mathbf{k}) = \frac{i}{2(\ln \kappa)} (\mathbf{p} \cdot \mathbf{E} \cdot \mathbf{p}) j_1(2\pi\mathbf{k} \cdot \mathbf{p}) \hat{\mathbf{G}}_0(\mathbf{k}) \cdot \mathbf{p}, \tag{3.5}$$

$$\hat{\mathbf{u}}(\mathbf{k}) = -\frac{i}{\ln \kappa} j_1(2\pi\mathbf{k} \cdot \mathbf{p}) (\hat{\boldsymbol{\Omega}} \wedge \mathbf{p}) \cdot \hat{\mathbf{G}}_0(\mathbf{k}), \tag{3.6}$$

where  $\mathbf{E}$  is the rate of strain tensor,  $j_1(z)$  is the spherical Bessel function of first order, and

$$\hat{\mathbf{G}}_0(\mathbf{k}) = \frac{1}{(2\pi)^2} \left( \frac{\mathbf{I}}{k^2} - \frac{\mathbf{k}\mathbf{k}}{k^4} \right), \tag{3.7}$$

is the Fourier transform of the Oseen tensor  $\mathbf{G}_0(\mathbf{r})$ . Substituting (3.5) and (3.6) in (3.4), and noting that the relation (2.9) holds for an arbitrary  $\hat{\boldsymbol{\Omega}}$ , one finally obtains

$$\dot{\mathbf{p}} = \boldsymbol{\Omega}_p \wedge \mathbf{p} = \boldsymbol{\Gamma} \cdot \mathbf{p} + \frac{3Re}{16\pi(\ln \kappa)} [(\mathbf{p} \cdot \mathbf{E} \cdot \mathbf{p})(\mathbf{J}_1 + \mathbf{J}_2) - \mathbf{J}_3], \quad (3.8)$$

where

$$\mathbf{J}_1 = \mathbf{p} \cdot \int \hat{\mathbf{G}}_0(\mathbf{k}) \cdot \boldsymbol{\Gamma}^\dagger \cdot \hat{\mathbf{G}}_0(\mathbf{k}) j_1^2(2\pi\mathbf{k} \cdot \mathbf{p}) \, d\mathbf{k}, \quad (3.9)$$

$$\begin{aligned} \mathbf{J}_2 = & \int \mathbf{k} \cdot \boldsymbol{\Gamma} \cdot \frac{\partial}{\partial \mathbf{k}} (j_1(2\pi\mathbf{k} \cdot \mathbf{p})) \hat{\mathbf{G}}_0(\mathbf{k}) \cdot \hat{\mathbf{G}}_0(\mathbf{k}) \cdot \mathbf{p} j_1(2\pi\mathbf{k} \cdot \mathbf{p}) \, d\mathbf{k} \\ & + \int \mathbf{k} \cdot \boldsymbol{\Gamma} \cdot \frac{\partial}{\partial \mathbf{k}} (\hat{\mathbf{G}}_0(\mathbf{k}) \cdot \mathbf{p}) \cdot \hat{\mathbf{G}}_0(\mathbf{k}) j_1^2(2\pi\mathbf{k} \cdot \mathbf{p}) \, d\mathbf{k}, \end{aligned} \quad (3.10)$$

$$\mathbf{J}_3 = \int \hat{\mathbf{G}}_0(\mathbf{k}) \cdot \frac{\partial}{\partial t} ((\mathbf{p} \cdot \mathbf{E} \cdot \mathbf{p}) j_1(2\pi\mathbf{k} \cdot \mathbf{p}) \mathbf{p}) \cdot \hat{\mathbf{G}}_0(\mathbf{k}) j_1(2\pi\mathbf{k} \cdot \mathbf{p}) \, d\mathbf{k}. \quad (3.11)$$

The integral  $\mathbf{J}_3$  arises due to the motion of the fibre, namely its changing orientation ( $\mathbf{p}(t)$ ), relative to the stationary (inertial) reference frame, leading to an unsteady disturbance velocity field in the Eulerian sense.

Before carrying out the detailed calculation of the integrals (3.9)–(3.11), we anticipate, using tensorial arguments, the general form for the leading-order inertial correction to the rate of change of fibre orientation. In the Stokes limit a fibre rotates as a material line element, leading to the Jeffery orbit equation:

$$\dot{\mathbf{p}}_{\text{jeff}} = \boldsymbol{\Gamma} \cdot \mathbf{p} - (\mathbf{E} : \mathbf{p}\mathbf{p})\mathbf{p}, \quad (3.12)$$

which is linear in the shear rate. Since the first effects of inertia may, in principle, be arrived at using a regular perturbation expansion, the leading inertial term will be  $O(Re)$  and a quadratic function of  $\mathbf{E}$  and/or  $\boldsymbol{\Omega}$ ,  $\boldsymbol{\Omega} = (\boldsymbol{\Gamma} - \boldsymbol{\Gamma}^\dagger)$  here being the vorticity tensor. The general form for such a term, excluding contributions arising from solid-body rotation, is given as

$$\begin{aligned} (p_{\text{corr}})_i = & \alpha_1 E_{ij} \Omega_{jk} p_k + \alpha_2 \Omega_{ij} E_{jk} p_k + \alpha_3 E_{ij} E_{jk} p_k \\ & + \alpha_4 (E_{kl} p_k p_l) \Omega_{ij} p_j + \alpha_5 (E_{kl} p_k p_l) E_{ij} p_j, \end{aligned} \quad (3.13)$$

where the  $\alpha_i$  are proportionality constants. Purely axial contributions of the form  $c\mathbf{p}$ ,  $c$  being a scalar, must be added in order for the fibre to be inextensible, i.e. for  $(\dot{\mathbf{p}}_{\text{jeff}} + Re \dot{\mathbf{p}}_{\text{corr}}) \cdot \mathbf{p} = 0$  to be satisfied; they do not lead to a change in orientation, however, and are therefore not included in (3.13). For a general linear flow, one can always choose a fibre-aligned orthogonal coordinate system (see figure 1) with the 1-direction along the fibre axis  $\mathbf{p}$ , and the 3-direction perpendicular to the vorticity vector ( $\boldsymbol{\omega}$ ). Thus,  $\mathbf{1}_3$  is directed along  $\boldsymbol{\omega} \wedge \mathbf{p}$ ; for simple shear, this constrains it to lie in the flow–gradient ( $XY$ ) plane. With this system of axes, elements such as  $\Omega_{23}$ ,  $E_{23}$  etc. are seen to drive fluid motion in a plane transverse to the fibre axis, leading to velocity disturbance fields that scale with the fibre diameter rather than its length, and are therefore not relevant in the slender-body approximation. With this restriction,  $\alpha_1 = \alpha_2 = \alpha_3 = 0$ . Finally, noting that  $\Omega_{21} = \omega_3 = 0$ , the components of the drift in the

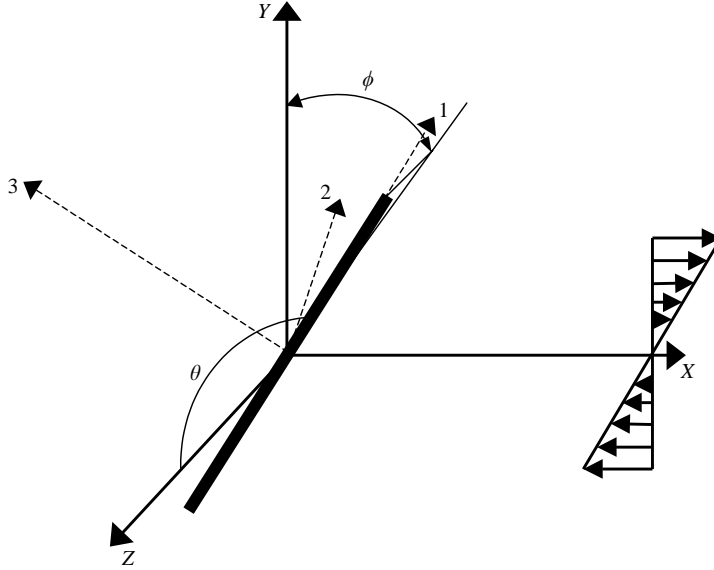


FIGURE 1. Coordinate system used for calculation of fibre drift in simple shear flow.

2- and 3-directions reduce to

$$\left. \begin{aligned} (\dot{p}_2)_{corr} &= \alpha_5 E_{11} E_{12}, \\ (\dot{p}_3)_{corr} &= E_{11} \left( \frac{\alpha_5 + \alpha_4}{2} \Gamma_{31} + \frac{\alpha_5 - \alpha_4}{2} \Gamma_{13} \right). \end{aligned} \right\} \quad (3.14)$$

The analysis that follows serves to determine the numerical value of the constants  $\alpha_4$  and  $\alpha_5$  in (3.14). We note that the coefficients of the three terms in (3.14) involve only two independent constants  $\alpha_4$  and  $\alpha_5$ , a fact that is borne out by the detailed form of the orbit equations derived below (see (3.20)).

In order to evaluate the  $J_i$ , we employ the fibre-aligned Cartesian coordinate system described above. The fibre orientation, relative to the original system of axes  $(XYZ)$ , is itself specified by angles  $\theta$  and  $\phi$ , where  $\theta$  is the polar angle between the fibre axis and the vorticity direction, and  $\phi$  is the dihedral angle between the gradient–vorticity and the fibre–vorticity planes. The above integrals can then be written in the following form:

$$(J_1)_i = \frac{4}{\pi^2} \int \left[ \frac{\Gamma_{i1}}{k^4} - \frac{(\Gamma_{ij}k_jk_1 + \Gamma_{j1}k_ik_j)}{k^6} + \frac{(E_{jk}k_jk_k)k_ik_1}{k^8} \right] j_1^2(2\pi k_1) \, d\mathbf{k}, \quad (3.15)$$

$$\begin{aligned} (J_2)_i &= \frac{2}{\pi^2} \int \left( \frac{\delta_{i1}}{k^4} - \frac{k_ik_1}{k^6} \right) \Gamma_{jk}k_j \frac{\partial}{\partial k_k} \{ j_1^2(2\pi k_1) \} \, d\mathbf{k} \\ &+ \frac{4}{\pi^2} \int k_j \Gamma_{jk} \left[ -\frac{(2\delta_{i1}k_k + \delta_{ik}k_1)}{k^6} + \frac{3k_ik_kk_1}{k^8} \right] j_1^2(2\pi k_1) \, d\mathbf{k}, \end{aligned} \quad (3.16)$$

$$\begin{aligned} (J_3)_i &= \frac{8}{\pi^2} E_{j1} \dot{p}_j \int \left( \frac{\delta_{i1}}{k^4} - \frac{k_ik_1}{k^6} \right) j_1^2(2\pi k_1) \, d\mathbf{k} + \frac{4}{\pi^2} E_{11} \dot{p}_j \int \left( \frac{\delta_{ij}}{k^4} - \frac{k_ik_j}{k^6} \right) j_1^2(2\pi k_1) \, d\mathbf{k} \\ &+ \frac{8}{\pi} E_{11} \dot{p}_m \int k_m \left( \frac{\delta_{i1}}{k^4} - \frac{k_ik_1}{k^6} \right) \left\{ \frac{j_1(2\pi k_1)}{2\pi k_1} - j_2(2\pi k_1) \right\} j_1(2\pi k_1) \, d\mathbf{k}, \end{aligned} \quad (3.17)$$



where the velocity gradient tensor in the fibre-aligned coordinate system is given by

$$\begin{aligned} \mathbf{\Gamma} &= \mathbf{1}_x \mathbf{1}_y, \\ &= \sin^2 \theta \cos \phi \sin \phi \mathbf{1}_1 \mathbf{1}_1 + \sin \theta \cos \theta \sin \phi \cos \phi (\mathbf{1}_1 \mathbf{1}_2 + \mathbf{1}_2 \mathbf{1}_1) \\ &\quad - \sin \theta \sin^2 \phi \mathbf{1}_3 \mathbf{1}_1 + \sin \theta \cos^2 \phi \mathbf{1}_1 \mathbf{1}_3 + \cos \theta \cos^2 \phi \mathbf{1}_2 \mathbf{1}_3 \\ &\quad - \cos \theta \sin^2 \phi \mathbf{1}_3 \mathbf{1}_2 + \cos^2 \theta \sin \phi \cos \phi \mathbf{1}_2 \mathbf{1}_2 - \sin \phi \cos \phi \mathbf{1}_3 \mathbf{1}_3. \end{aligned} \tag{3.18}$$

In order to evaluate the leading-order inertial correction, it suffices to use the Stokes expression for  $\dot{\mathbf{p}}$  in  $\mathbf{J}_3$ , namely (3.12), this being equivalent to regarding the Eulerian acceleration of the velocity field ( $\partial \mathbf{u} / \partial t$ ) as arising from the rotation of the slender fibre as if it were a fluid line element. Carrying out the integrations analytically in Fourier space, the following equations characterize the fibre orbits to  $O(Re)$  in the limit of large aspect ratio:

$$\left. \begin{aligned} \dot{p}_2 &= E_{12} + \frac{28\pi Re}{15 \ln \kappa} E_{11}, \\ \dot{p}_3 &= \Gamma_{31} + \frac{Re}{\ln \kappa} E_{11} \left( \frac{4\pi}{3} \Gamma_{31} + \frac{8\pi}{15} \Gamma_{13} \right), \end{aligned} \right\} \tag{3.19}$$

where we have written down only the ‘2’ and ‘3’ components of (3.8) since the component in the ‘1’-direction merely serves to satisfy the inextensibility constraint. Using (3.18) for the components of  $\mathbf{\Gamma}$  and  $\mathbf{E}$ , one then obtains

$$\left. \begin{aligned} \dot{p}_2 = \dot{\theta} &= \sin \theta \cos \theta \sin \phi \cos \phi \left( 1 + \frac{28\pi Re}{15 \ln \kappa} \sin^2 \theta \sin \phi \cos \phi \right), \\ \frac{\dot{p}_3}{\sin \theta} = \dot{\phi} &= -\sin^2 \phi - \frac{Re}{\ln \kappa} \sin \theta \sin \phi \cos \phi \left( \frac{4\pi}{3} \sin \theta \sin^2 \phi - \frac{8\pi}{15} \sin \theta \cos^2 \phi \right). \end{aligned} \right\} \tag{3.20}$$

### 3.1.2. Analysis of the fibre orbit equations

The structure of the orbit equations (3.20) resembles that of similar equations derived for the motion of a torque-free fibre in the shearing flow of a second-order fluid (see Leal 1975). The inertial terms in (3.20) are, in fact, identical in form to the non-Newtonian correction terms found by Leal, except for the opposing signs. It was shown earlier in this section, using general continuum mechanics arguments, that this similarity arises because terms representing the first effects of inertia and elasticity in simple shear flow are both quadratic functions of  $\mathbf{E}$  and  $\mathbf{\Omega}$ , and reduce to the same tensorial form in the slender-body limit. The resulting alteration of the fibre motion due to fluid inertia for small  $Re$  is thus qualitatively similar to that induced by weak elasticity but opposite in sense.

For  $Re = 0$ , the system (3.20) can be integrated to obtain

$$\cot \phi = t, \quad \tan \theta = C / \sin \phi, \tag{3.21}$$

showing that the slender-fibre trajectories, at leading order, are identical to those of a fluid line element in simple shear flow when projected onto the unit sphere. As shown in figure 2, they coincide with the meridians of the unit sphere with the flow direction as its polar axis. Here,  $C$  is the orbit constant;  $C = \infty$  represents motion in the flow-gradient plane, while  $C = 0$  corresponds to the degenerate set of fibre orientations in the flow-vorticity plane. Note that neglect of the finite thickness of the fibre, and thence the  $O(\kappa^{-2})$  torque responsible for fibre rotation through the flow-aligned state (see discussion below), leads to trajectories that are no longer closed orbits; in fact,

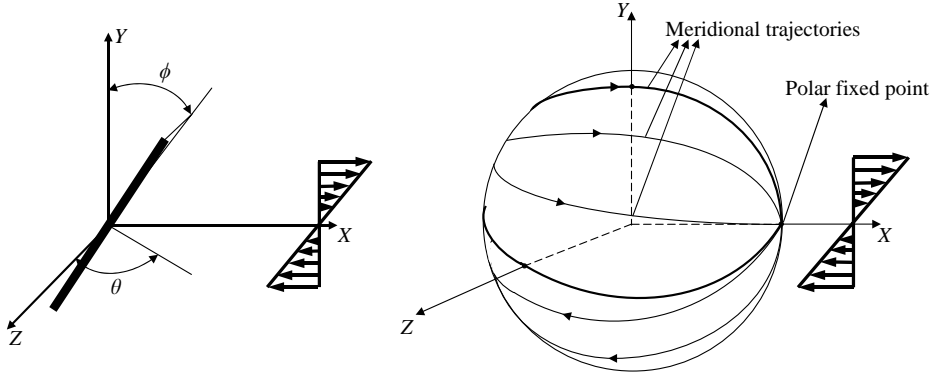


FIGURE 2. The meridional trajectories of a line element (slender fibre) in simple shear flow. The flow–vorticity plane comprises a degenerate set of stationary fibre orientations.

for almost all initial orientations, the slender fibre eventually aligns itself with the flow axis.

For small but finite  $Re$ , it is convenient to recast (3.20) in terms of the natural  $(C, \tau)$  coordinate system (see Leal & Hinch 1971),  $\tau = \cot \phi$  being the orbit phase; one obtains

$$\frac{d\tau}{dt} = 1 + \frac{\pi Re}{\ln \kappa} \frac{\sin^2 \theta \cos \phi}{\sin \phi} \left( \frac{4}{3} \sin^2 \phi - \frac{8}{15} \cos^2 \phi \right), \tag{3.22}$$

$$\frac{dC}{dt} = \left[ \frac{8\pi Re}{15 \ln \kappa} \sin^2 \theta \cos^2 \phi \right] C. \tag{3.23}$$

From (3.23), evidently  $C \rightarrow \infty$  as  $t \rightarrow \infty$ , and thus, the first effect of fluid inertia is to induce an  $O(Re)$  drift that, in the slender-body approximation, drives the fibre towards the flow–gradient plane.

We now examine the system (3.20) in more detail. Figure 3(a) shows both the inertialess and  $O(Re)$  modified trajectories on a (small) portion of the unit sphere surrounding the flow axis, i.e. for  $(\theta, \phi) \approx (\pi/2, 0)$ . Locally, the surface of the unit sphere may then be replaced by its tangent plane – the  $(y, z)$ -plane in this case, with  $y(\approx \phi)$  and  $z(\approx \pi/2 - \theta)$  being the local coordinates in the gradient and vorticity directions, respectively, and the origin corresponding to the intersection of the unit sphere with the flow direction. For zero inertia, the orbit equations on this tangent plane reduce to the following approximate form:

$$\frac{dy}{dt} \approx -y^2, \tag{3.24}$$

$$\frac{dz}{dt} \approx -yz. \tag{3.25}$$

The  $z$ -axis (the flow–vorticity plane) represents a continuum of fixed points for the above system. Solving (3.25), one obtains  $dy/dz = y/z$ ; the resulting trajectories, depicted by dashed lines in the figure, are locally radial, with the trajectories for  $y > 0$  asymptotically approaching the origin, and those with  $y < 0$  diverging from it. This is, of course, consistent with the meridional nature of the inertialess fibre trajectories seen above. For small but finite  $Re$ , the local representation of the orbit equations is

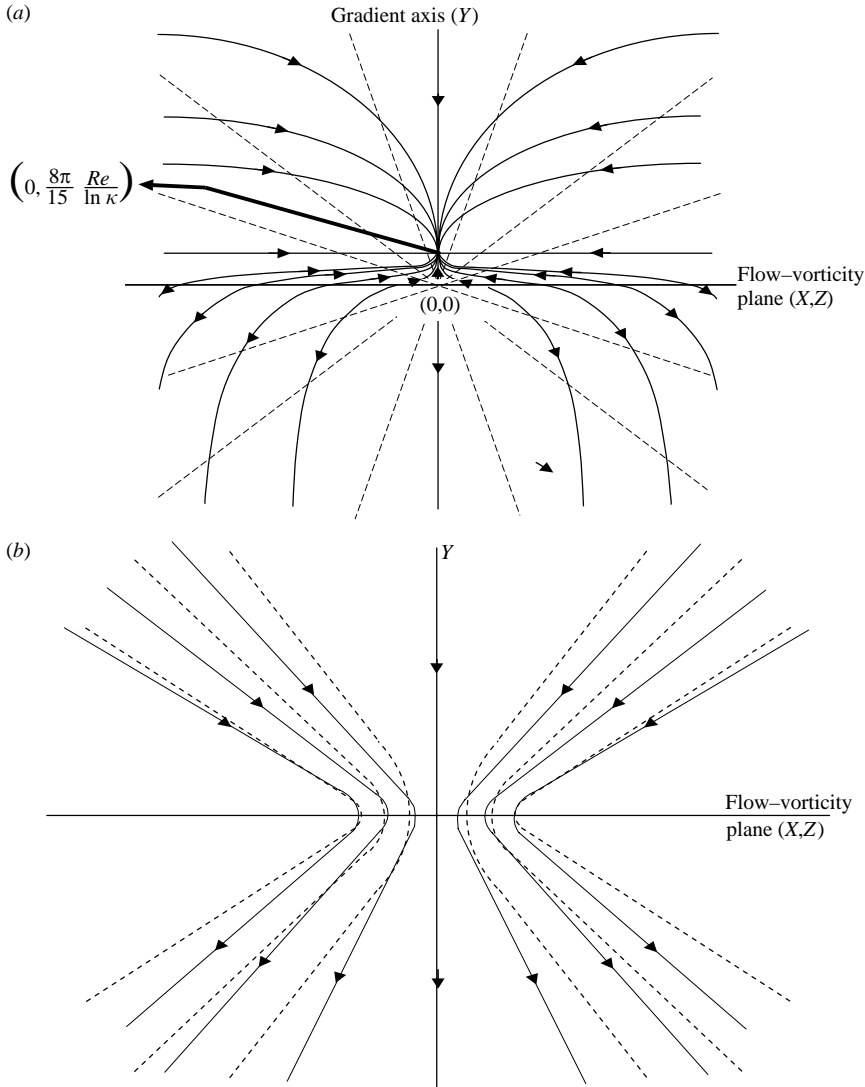


FIGURE 3. (a) The modified inertial trajectories (solid lines) of a slender fibre in simple shear flow on a magnified section of the unit sphere, when viewed along the flow direction. For comparison, the inertialess trajectories are shown by dashed lines. The latter, being of a meridional character, are radial in this viewpoint, converging toward the intersection of the unit sphere with the flow axis. The inertial trajectories cross successive meridians, eventually asymptoting to  $y = (8\pi/15)Re/\ln \kappa$  on the flow-gradient plane. (b) Modified inertial trajectories for a fibre of finite aspect ratio, again viewed along the flow axis. The inertialess trajectories, again depicted by dashed lines, are now closed orbits that cross the flow-vorticity plane; the inertial trajectories are again seen to cross Jeffery orbits en-route to the flow-gradient plane.

given by

$$\frac{dy}{dt} \approx -y^2 + \left(\frac{8\pi}{15}\right) \left(\frac{Re}{\ln \kappa}\right) y, \tag{3.26}$$

$$\frac{dz}{dt} \approx -yz, \tag{3.27}$$

at leading order. Thus, in addition to the  $z$ -axis, the system (3.27) now has a fixed point at  $(y, z) \equiv [(8\pi/15)Re/\ln\kappa, 0]$ ; this point corresponds to the fibre orientation  $(\theta, \phi) = [\pi/2, (8\pi/15)Re/\ln\kappa + o(Re)]$  for the full system (3.20). It is easily shown that the fixed points on the  $z$ -axis are all unstable; for instance, the  $y$ -axis is an unstable manifold for the origin. On the other hand,  $[(8\pi/15)Re, 0]$  represents a stable fixed point. The resulting inertial trajectories are also depicted in figure 3(a) by solid lines. Each inertial path is seen to cross successive inertialess meridional trajectories (dashed lines), finally approaching the fixed point  $[(8\pi/15)Re, 0]$  in a direction tangent to the flow-gradient plane. The configuration of trajectories in a region close to the other pole  $(\theta, \phi \rightarrow \pi/2, \pi)$  of the unit sphere is obtained by reflection of the depicted trajectory topology with respect to the flow-vorticity plane, as is required by the antisymmetry of simple shear. For finite  $Re$ , almost all initial orientations eventually approach the flow-gradient plane at an inclination of  $\phi \approx (8\pi/15)Re/\ln\kappa$ .

Equations (3.20) govern the trajectories of a slender fibre only in the limit of infinite aspect ratio. Since a flow-aligned fibre does not rotate in this limit, the inertial torque in (3.20) always dominates for small enough  $\phi$ , leading to the aforementioned stationary orientation in the flow-gradient plane. However, an inertialess fibre with a large but finite aspect ratio experiences a small  $O(\kappa^{-2})$  torque even in the flow-aligned position, and thus rotates in a closed (Jeffery) orbit, spending only an  $O(1/\kappa)$  fraction of the time in orientations with  $\phi > 1/\kappa$ .<sup>†</sup> In order to achieve this periodic flipping exhibited by actual fibres, one must incorporate the  $O(\kappa^{-2})$  angular velocity arising from the finite fibre diameter in the equation for  $\dot{\phi}$  in (3.20). One of the consequences of including the aforementioned correction is that, for small enough  $Re$ , the fibre continues to rotate across the flow-vorticity plane, and a stationary orientation does not arise until a certain critical Reynolds number that is calculated below; the equation for  $\dot{\phi}$  now takes the form

$$\dot{\phi} = \frac{-1}{(\kappa_e^2 + 1)} (\kappa_e^2 \sin^2 \phi + \cos^2 \phi) - \frac{Re}{\ln \kappa} \sin \theta \sin \phi \cos \phi \left( \frac{4\pi}{3} \sin \theta \sin^2 \phi - \frac{8\pi}{15} \sin \theta \cos^2 \phi \right). \quad (3.28)$$

Note that the equation for  $\dot{\theta}$  in (3.20) still remains unaltered at leading order for large  $\kappa$ . The orbit constant, now defined for a finite aspect ratio, is  $C = \tan \theta \sin \phi (1 + \kappa_e^{-2} \cot^2 \phi)^{1/2}$ , with  $C = 0$  corresponding uniquely to the vorticity axis. Here, and in (3.28),  $\kappa_e = \beta\kappa$  is an equivalent aspect ratio, the proportionality factor  $\beta$  being only a weak function of  $\kappa$  (see Cox 1971); experiments with rod-like particles with aspect ratios in the range 10–100 have shown  $\beta$  to be close to 0.7 (Anczurowski & Mason 1967). Thus, with the above modification, the inertialess meridional trajectories become closed Jeffery orbits, and the  $O(Re)$  crossing of meridians seen earlier translates to migration across Jeffery orbits with increasing orbit constants towards an eventual tumbling motion in the flow-gradient plane. Figure 3(b) shows these spiralling trajectories when viewed along the flow axis, and

<sup>†</sup> This  $O(\kappa^{-2})$  torque is related to the finite fibre diameter and cannot be obtained by regarding the fibre as a line distribution of forces, as was assumed earlier. The latter distribution is, in fact, identically zero to all orders in  $(\ln \kappa)^{-1}$  for the flow-aligned orientation. A fibre in this orientation acts, at leading order, as a distribution of force-dipoles, leading to a torque that is algebraically smaller, being of  $O(\kappa^{-2})$ ; for blunt-edged bodies, the contribution to this torque comes from the blunt ends, and thereby precluding the use of slender-body theory (see Cox 1971).

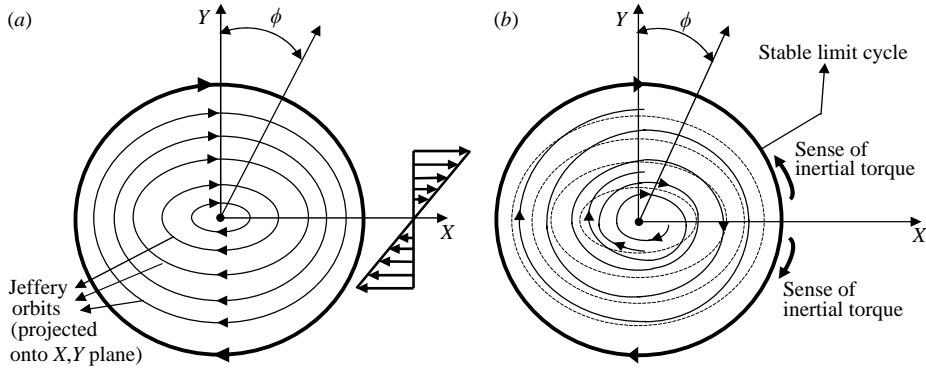


FIGURE 4. (a) The Jeffery orbits of a finite-aspect-ratio fibre when projected onto the flow–gradient plane. The  $O(Re)$  corrected behaviour of the trajectories: inertial trajectories spiral out crossing successive Jeffery orbits (dotted lines) approaching the stable limit cycle in the shearing plane.

may be contrasted with the trajectory configuration in the limit of infinite aspect ratio illustrated in figure 3(a). For  $Re$  small enough, the surface of the unit sphere thus transforms from a structurally unstable centre manifold at  $Re = 0$  to a structurally stable combination of an attracting limit cycle (the flow–gradient plane) and a pair of spiral repellers (the intersections of the vorticity axis with the unit sphere) for small but finite  $Re$  (see figure 4).

The evolution of the orbit constant calculated using (3.28) is shown in figure 5, where we have plotted the ratio  $C/(C + 1)$  as a function of time for a fibre aspect ratio  $\kappa = 20$ , and for  $Re = 0.05$ . The dominant changes are seen to occur in the nearly aligned phases of the Jeffery orbits, with  $\phi$  near  $n\pi$ , where the fibre spends the most time, and for which case the inertial drift in (3.23) attains its maximum value. The otherwise monotonic increase in  $C/(C + 1)$  is modulated by a secondary wiggle on the scale of a Jeffery period, leading to a pair of short plateaus in a  $\pi$  interval of  $\phi$ . One of these plateaus, the shorter one, arises because the orbit constant remains virtually unchanged during the  $O(\dot{\gamma}^{-1})$  time the fibre takes to rotate through orientations with  $|\phi|, |\pi - \phi| \gg O(1/\kappa)$ . As the fibre approaches flow alignment, i.e. when  $0 < \phi < O(1/\kappa)$  or  $\pi < \phi < \pi + O(1/\kappa)$ , the orbit constant starts to increase and the increase continues for a time of  $O(\kappa \dot{\gamma}^{-1})$  until the inertial angular velocity in (3.28) becomes much smaller than the  $O(\kappa^{-2})$  contribution associated with the finite fibre diameter. The fibre then rotates through the aligned position in a time of  $O(\kappa \dot{\gamma}^{-1})$ , again with little change in the orbit constant, leading to the second, longer, plateau. This is followed by a second long  $O(\kappa \dot{\gamma}^{-1})$  period of increase as the fibre rotates out of alignment. The change in the sign of the inertial angular velocity across the flow axis implies that the magnitudes of increase in the orbit constant in these intervals differ for any finite  $Re$ .

From (3.28), it is easily seen that the inertial correction vanishes at  $\phi_c \sim \tan^{-1}[\pm(2/5)^{1/2}]$ , the fibre in this orientation rotating with an angular velocity identical to its inertialess value. For  $\phi_c < \phi < \pi/2$ , the fibre rotates faster than at  $Re = 0$ , whereas it is decelerated by inertial forces in the region  $0 < \phi < \phi_c$ . As a result, a fibre at finite  $Re$  rotates into the flow-aligned state ( $\phi = 0$ ) slower than at  $Re = 0$ , but moves out of alignment slightly faster. Since the  $O(Re)$  inertial torque opposes the (small) leading-order Jeffery rotation for a fibre moving into alignment, the possibility of a ‘non-rotating’ mode arises (by ‘non-rotating’, here, we mean that

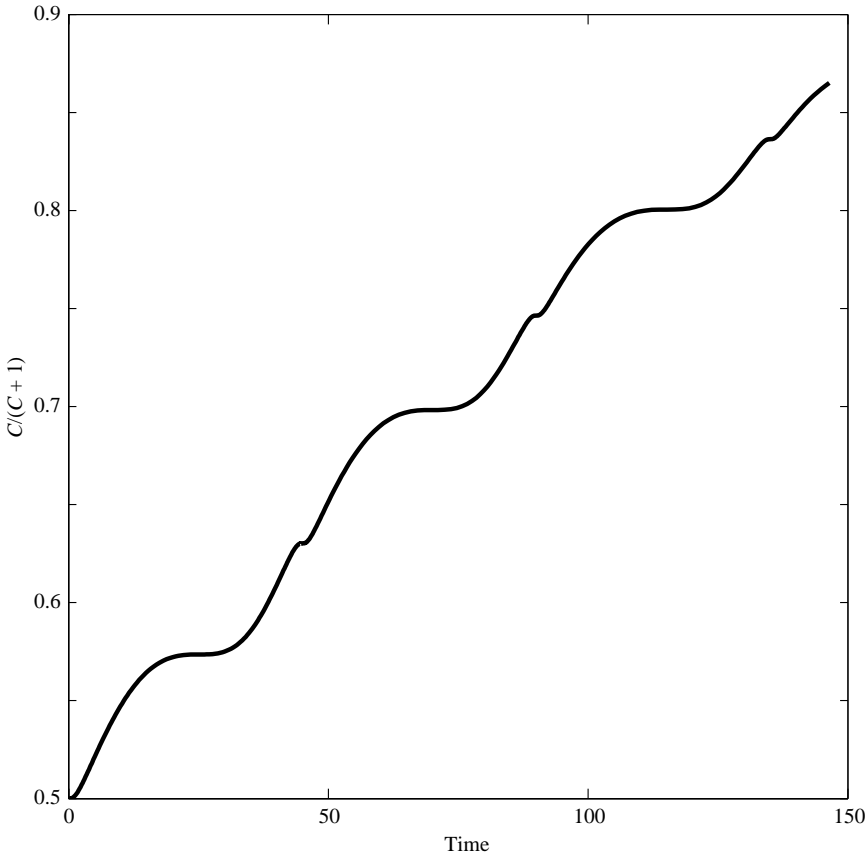


FIGURE 5. The ratio  $C/(C + 1)$ ,  $C$  being the orbit constant as a function of time (scaled with the shear rate), for  $Re = 0.05$  and a fibre aspect ratio of 20.

the fibre no longer undergoes Jeffery-like rotations with  $\phi$  being a periodic function of time; both values of  $\theta$  and  $\phi$  continue to change as the fibre asymptotes towards a fixed orientation in the shearing plane). With  $Re \ll 1$  the orientation of this stationary state, as seen in the flow–gradient plane, may be determined from the limiting form of (3.28) for  $\phi \rightarrow 0$ :

$$\dot{\phi} = -\phi^2 - \frac{1}{\beta^2 \kappa^2} + \frac{8\pi Re}{15 \ln \kappa} (\sin^2 \theta) \phi. \tag{3.29}$$

Equating  $\dot{\phi}$  to zero leads to a quadratic equation for  $\phi$ , only one of whose roots yields a stable fixed point. The stable fixed point reduces to  $\phi = (8\pi/15)Re/\ln \kappa$ , and the unstable one to the flow–vorticity plane, for an infinitely thin fibre, this then being consistent with the behaviour predicted by (3.20). Solving (3.29), the stable orientation for a finite-aspect-ratio fibre is given by

$$\phi_f = \frac{4\pi Re}{15 \ln \kappa} \sin^2 \theta + \left\{ \frac{16\pi^2 Re^2}{225(\ln \kappa)^2} \sin^4 \theta - \frac{1}{\beta^2 \kappa^2} \right\}^{1/2}. \tag{3.30}$$

This stationary orientation is physically realizable when (3.30) is real valued, that is, provided  $Re > Re_c$  with

$$Re_c = (15/4\pi)(\ln \kappa / \beta \kappa) \sin^{-2} \theta, \tag{3.31}$$

this being a fairly modest value for sufficiently large-aspect-ratio fibres. For  $Re$  not much larger than the critical value,  $\phi_f \sim O(\kappa^{-1})$ .

From the expression for  $Re_c$  it is seen that the critical shear rate increases with decreasing  $\theta$ . A fibre that first becomes stationary at a given shear rate, and for a specific value of  $\theta$ , will therefore drift towards the plane of shear without further rotation, the increase in  $\theta$  accompanying this drift ensuring that the stationary states en-route remain physically realizable. This is in contrast to Leal's predictions for fibre motion in a second-order fluid (see Leal 1975). In this latter case, the domain of stationary states for any finite shear rate does not include the vorticity axis, and thus, the eventual approach towards vorticity alignment is always via a spiralling trajectory, a behaviour supported by experiments (see Bartram, Goldsmith & Mason 1975). Our analysis is consistent, at least in part, with earlier experiments by Karnis, Goldsmith & Mason (1966) who investigated the orientational behaviour of rods and disks in Poiseuille and Couette flow in the presence of inertial effects. In particular, they found neutrally buoyant rods in the latter to steadily drift over many rotations, eventually tending toward the  $C = \infty$  orbit in the shearing plane. The highest shear rate used in the experiments was  $11.6 \text{ s}^{-1}$  for a system of aluminium-coated Nylon rods with aspect ratio  $\kappa \sim 10$  in a fluid mixture with  $\rho = 1.09 \text{ g cm}^{-3}$  and  $\mu = 1.2 \text{ P}$ . The Reynolds number for this system is around 0.1, while the critical value for the existence of a non-rotating mode is found to be approximately 0.35, using (3.31) and taking  $\beta$  to be around 0.8 (as also found by the above authors). Thus, the experimental findings agree with the predicted drift towards the plane of shear for  $Re < Re_c$ . Verification of the predictions for  $Re > Re_c$  would require experiments at higher shear rates, and possibly in a less viscous fluid. Visualization experiments carried out in rheological apparatus, in this latter regime, must be performed with care to ensure that secondary flow effects remain minimal with increasing shear rate.

### 3.2. Physical mechanism for fibre drift

We now examine the physical origin of the changes in orbit constant and phase, first noting that the unsteadiness of the disturbance velocity field ( $\partial \mathbf{u}' / \partial t$ ) is not essential to the governing physics of the orbital drift. This may be seen, in part, from (3.23) and (3.22) wherein the inertial corrections attain their greatest values with the fibre nearly aligned with the flow direction, when its angular velocity is the smallest. Unsteady effects are evidently minimized in such a case. More fundamentally, the symmetry of the leading-order quasi-steady disturbance velocity field about the fibre-flow plane implies that Eulerian unsteadiness by itself, while affecting the orbit phase (and thus, the precise value of  $\phi_c$ ), will not induce a motion orthogonal to the fibre-flow plane, leaving the orbit constant unchanged in the slender-body limit. We therefore base our physical arguments on the quasi-steady disturbance velocity field.

The instantaneous streamlines in the fibre-flow plane ( $\psi = \text{constant}$ ) for fluid motion around the slender fibre are shown in Figs 6 and 7. In figure 6 where  $\phi < \phi_c < \pi/2$ , the perturbed streamlines meet the fibre at right angles to its length, satisfying the boundary condition of solid-body rotation; the directions of the inertial forces ( $\propto \mathbf{u} \cdot \nabla \mathbf{u}$ ) resulting from the streamline curvature are indicated by the little arrows. The tighter spacing of streamlines on the side where the fibre makes an acute angle with the flow axis implies an acceleration of the fluid here relative to the obtuse-angled region, so the corresponding point forces are greater in magnitude, indicated by longer arrows in the figure. The heavy curved arrows represent the sense of the net torque that arises. This torque, projected onto the flow-gradient plane, is consistent with the inertial modification of orbit phase in the region  $\phi_c < \phi < \pi/2$  discussed

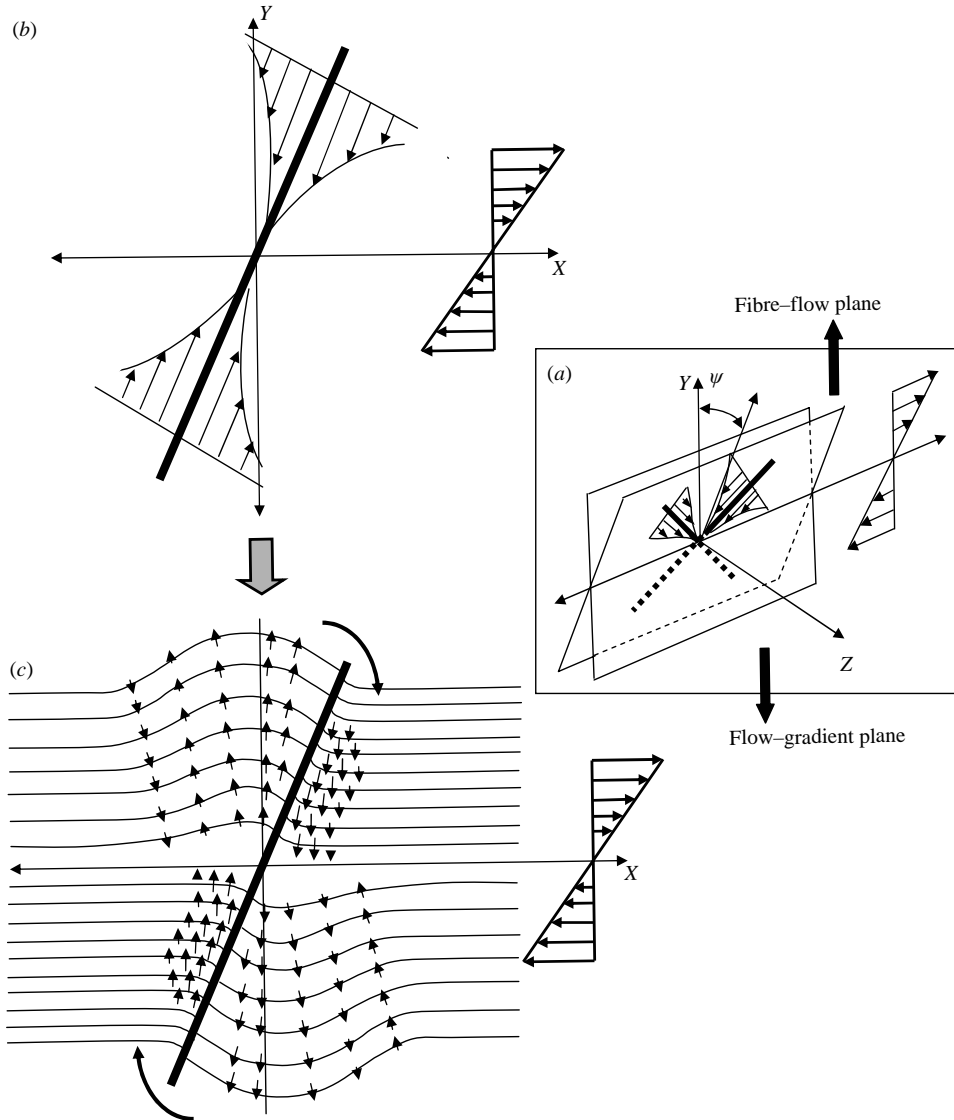


FIGURE 6. (a) The boxed figure depicts the fibre-flow plane and the dihedral angle  $\psi$  it makes with the plane of shear. The disturbance velocity field of the fibre in the fibre-flow plane is shown on (b) for an orientation with  $\phi > \phi_c$ . (c) The resulting streamlines, again in this plane, and the resulting array of inertial point forces. The sense of the net inertial torque is shown by the two curved arrows.

above. For an orientation that is a mirror image with respect to the gradient axis (i.e.  $\pi/2 < \phi < \pi - \phi_c$ ), the fibre is in the compressional quadrant of simple shear, the disturbance velocity field now changing character from biaxial to uniaxial extension along the fibre; the regions of acceleration and deceleration, being decided by the angle between the fibre and the flow axis, are now interchanged leading to a torque in the opposite sense. In figure 7 the fibre is shown immediately prior to crossing the flow axis. The forces induced on the fibre on account of its inextensibility, in this nearly aligned orientation, lead to a velocity field that accelerates the fluid in



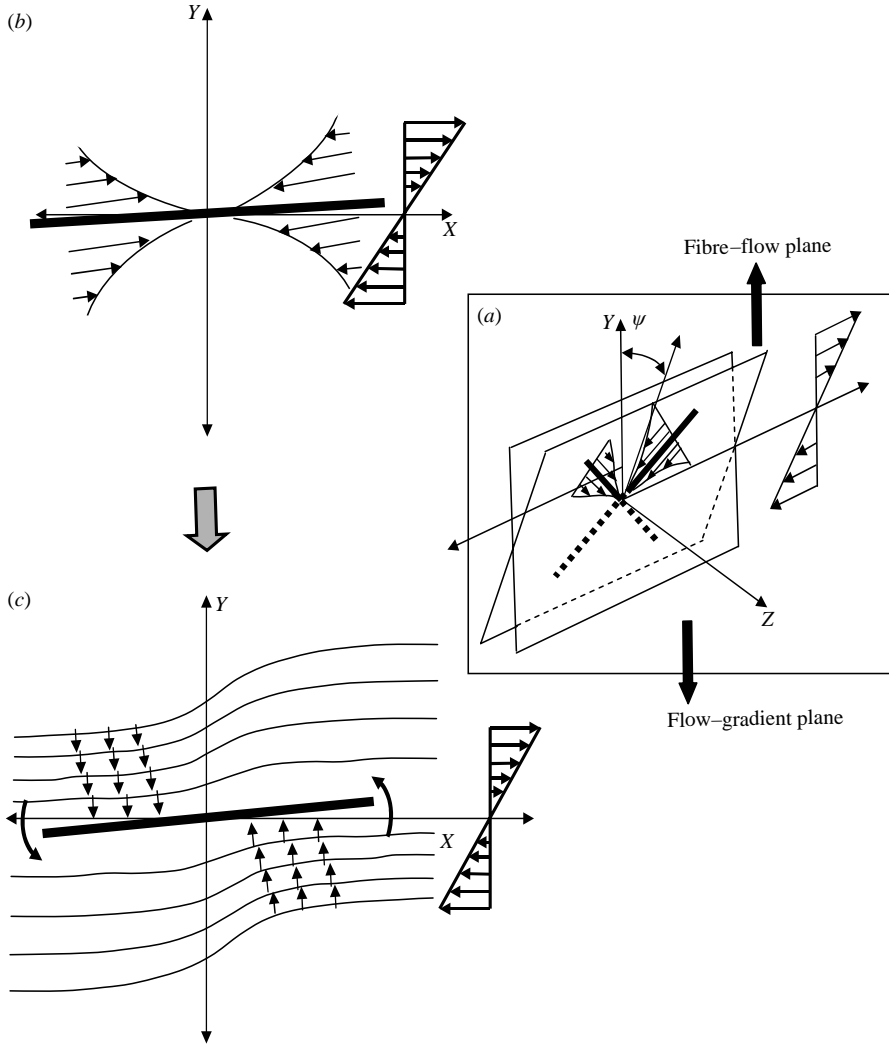


FIGURE 7. As figure 6 but for an orientation with  $\phi \rightarrow 0$ .

regions corresponding to  $\phi \sim 0^-$  and  $\phi \sim \pi^-$ , in turn leading to a torque that retards alignment. This retardation is again in agreement with the analysis in the preceding paragraphs, and is responsible for the emergence of a stationary state for  $Re > Re_c$ .

To analyse the change in orbit constant due to migration across inertialess meridional trajectories, it is necessary to consider fluid motion induced orthogonal to the fibre-flow plane. For purposes of the following qualitative reasoning, that serves to determine the direction of the  $O(Re)$  drift, the fibre may be treated as a dumbbell comprising a pair of oppositely directed point forces, proportional to the local slip velocity, and displaced from one another by a distance of  $O(l)$  (see figure 8). The similarity of a fibre and a dumbbell at low  $Re$  can, in fact, be made quantitative. An analysis for a torque-free dumbbell in simple shear is virtually identical to the one carried out above, the only difference being that the spherical Bessel function corresponding to the fibre forcing in Fourier space is now replaced by an elementary sine function. It yields orbit equations of the same form, differing only in the values of

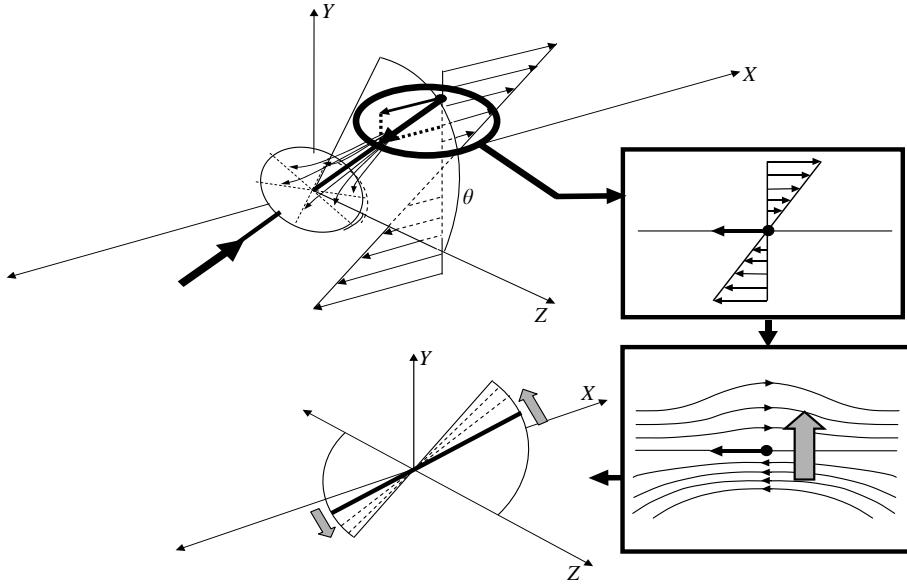


FIGURE 8. The induced velocity disturbance due to the dumbbell in simple shear flow. The two insets show the directions of the inertial lift forces acting on one of the point forces comprising the dumbbell on account of streamline curvature.

the numerical constants. Thus the aforementioned conclusions with regard to change in both orbit constant and phase remain unchanged for a dumbbell in the limit  $Re \ll 1$ . This analogy of a fibre with a dumbbell is, of course, valid with regard to the nature of the respective disturbance velocity fields at distances of order  $O(l)$  or greater. The near-field behaviour of the velocity fields, i.e. for distances  $r \ll l$  from the point forces of the dumbbell or for  $r \sim O(d)$  from the fibre axis, is very different; that for a fibre is logarithmic, characteristic of Stokes flow in two dimensions, while that close to the individual point forces in the dumbbell diverges as  $1/r$ . In either case, however, the near-field contributions to the inertial torque are negligibly small, and are therefore not relevant to the argument that follows. Returning to figure 8, we first observe that owing to the antisymmetry of simple shear, the sense of the inertial couple can be deduced by considering the nature of the perturbed streamlines around only one of the two point forces. Further, as shown in figure 8, it suffices to consider the component of the point force in the flow direction, the effect of the gradient component being restricted to the fibre-flow plane. The flow component accelerates the ambient simple shear on one side relative to the other, leading to curved streamlines of the form shown in the inset. The nature of curvature clearly points to a resultant lift force in the positive gradient direction. The component of this lift force perpendicular to the fibre-flow plane, together with its antisymmetric counterpart, constitute the inertial couple. For an orientation that is a mirror image with respect to the gradient-vorticity plane, the forces exerted by the dumbbell reverse direction, the fibre being in the compressional quadrant. The direction of the inertial lift forces, and sense of the resulting couple, remain unchanged. The  $O(Re)$  component of  $\theta$  therefore has the same (positive) sign in the quadrants  $\phi \in (\pi/2, \pi)$  and  $\phi \in (0, \pi/2)$ , while that of  $\dot{\phi}$  reverses sign from being negative for  $\phi$  close to  $\pi/2$  to being positive for small  $\phi$  or  $(\pi - \phi)$ . Both of these are consistent with migration towards the flow-gradient plane ( $\theta = \pi/2$ ).

#### 4. Comparison with previous work

It was seen in the previous section that the motion of a fibre and a dumbbell are qualitatively similar in the limit of small  $Re$ . Harper & Chang (1968) analysed the motion of a dumbbell shaped particle in simple shear in the limit when the separation  $l$  of the spheres comprising the dumbbell is much greater than the inertial screening length  $(\nu/\dot{\gamma})^{1/2}$ , i.e. when  $Re$  as defined above is asymptotically large. An  $O(\epsilon^2 Re^{1/2})$  torque, assumed to result from Saffman-like lift forces (see Saffman 1965 and below) acting independently on the individual spheres, was found to move the dumbbell towards the plane of shear;  $\epsilon = a/l$  is the ratio of the sphere radii to their separation. Re-examining the physical situation as well as the assumptions underlying this analysis reveals, however, inconsistencies that severely restrict its applicability.

In order to determine the precise regime of validity for Harper & Chang's prediction, it is necessary to consider Saffman's original work, wherein he obtained an expression for the inertial lift on a sphere moving in simple shear, with a slip velocity  $U$  directed along the ambient streamlines, under the assumption  $U \ll (\nu\dot{\gamma})^{1/2}$ . For a freely rotating dumbbell of length  $l$ , the slip velocity of the spheres is  $O(\dot{\gamma}l)$  for orientations not too close to either the gradient axis or the flow-vorticity plane. The equivalent assumption for either sphere in the dumbbell would be  $\dot{\gamma}l \ll (\nu\dot{\gamma})^{1/2}$  or  $Re \ll 1$ , in direct contradiction to the intended limit. Indeed, on length scales of  $O(\nu/\dot{\gamma})^{1/2}$ , where the lift force originates, the dumbbell acts as a force-dipole rather than a point force (as in Saffman's analysis), and the corresponding contribution from this Oseen region is weaker, being only  $O(Re^{3/2})$  (see § 3.1). Therefore, deriving a lift force on one sphere under Saffman's original assumption, while neglecting the other, is clearly incorrect. For orientations nearly aligned with the flow-vorticity plane, however, the slip velocity  $V \sim O(\dot{\gamma}l\phi)$ , so that a necessary condition for the validity of the Harper & Chang analysis is  $\phi \ll Re^{-1/2}$ .† In the limit  $l \ll (\nu/\dot{\gamma})^{1/2}$ , the velocity disturbance due to the individual spheres decays rapidly everywhere beyond the (small) inertial screening length, except in the wake. Since their analysis assumes that the two spheres do not interact hydrodynamically, we further require that one sphere not be in the wake of the other. The wake region in simple shear has an antisymmetric structure as shown in figure 9 and grows like  $(\nu x/\dot{\gamma})^{1/3}$ , thereby excluding orientations in the flow-vorticity plane close to the flow axis. The final domain of validity is found to be  $\phi \ll Re^{-1/2}$ ,  $\pi/2 - \theta \gg Re^{-1/3}$ , the latter restriction precluding the region  $\pi/2 - \theta \sim O(a/l)$  where most Jeffery orbits with orbit constants  $C \geq O(1)$  cross the flow-vorticity plane.

It is worth emphasizing that the underlying physical mechanisms for the fibre drift toward the flow-gradient plane, even in the narrow angular range above, are very different for  $Re \ll 1$  and  $Re \gg 1$ . In the former case, as was shown in § 3, the  $O(Re)$  migration results from inertial forces in the viscous-dominated region of  $O(l)$ , while lift forces comprising the inertial couple for  $Re \gg 1$  have their origin in the well-known inviscid mechanism operating in the region  $r \gg (\nu/\dot{\gamma})^{1/2}$ . This fact is not explicitly mentioned in the literature, and we therefore digress briefly to elaborate on the lift-force scaling found by Saffman (1965). A particle of radius  $a$ , translating with velocity  $U$  relative to a simple shear flow, in the limit  $Re_a = a^2\dot{\gamma}/\nu \ll 1$ , 'carries' with

† The slip velocity is also vanishingly small for orientations close to the gradient-vorticity plane, being of  $O[\dot{\gamma}l(\pi/2 - \phi)^2]$ ; Harper & Chang's analysis is therefore also valid when  $(\pi/2 - \phi) \ll Re^{-1/4}$ . This regime is of little interest since the inertial corrections become significant only for nearly flow-aligned orientations when the leading-order angular velocity is small.

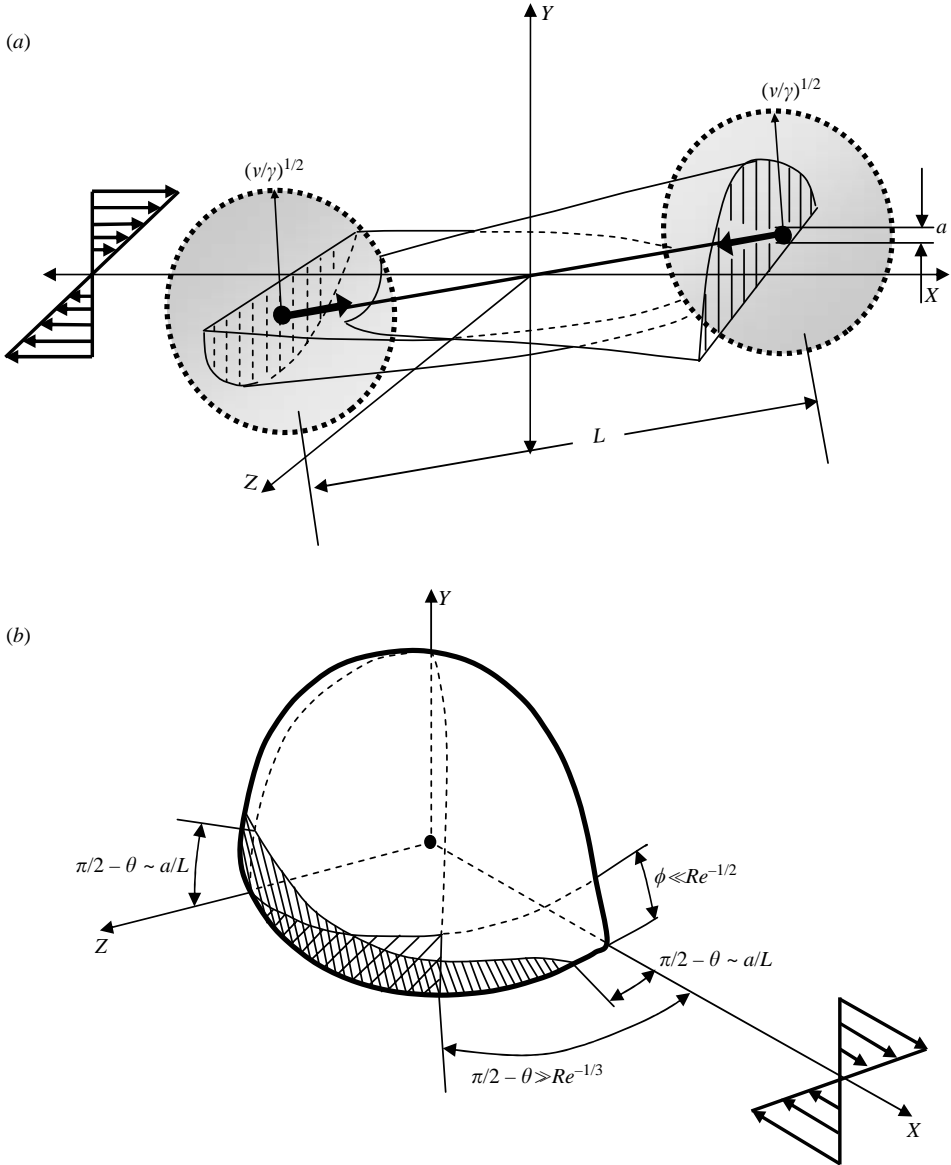


FIGURE 9. (a) The wake regions of the two spheres comprising the dumbbell, and the resulting shielding effect. (b) The restricted regime of validity for Harper & Chang's analysis; the only overlap is with the vanishingly small region of Jeffery orbits with orbit constants  $C < O(1)$ .

it a large fluid sphere of radius  $(\nu/\dot{\gamma})^{1/2}$ , this being the extent of the inner Stokes region where the velocity disturbance decays viscously, provided  $\nu/U \gg (\nu/\dot{\gamma})^{1/2}$ . The Magnus lift force mechanism, originating in the outer region at length scales of  $(\nu/\dot{\gamma})^{1/2}$  or greater, acts on this fluid sphere, endowing it with a transverse velocity of  $O(U)$ . This transverse outer velocity field forces the first-order inertial correction in the inner region. For a point force in simple shear, the latter is known to grow like  $r$  with distance  $r$  away from the particle; the resulting magnitude of the transverse velocity at the surface of the particle is therefore correspondingly smaller, being of

$O[(a^2\dot{\gamma}/\nu)^{1/2}U]$ , in turn leading to a lift force of  $O(\mu a U Re_a^{1/2})$ , identical to the original result derived by Saffman.

Evidently, the case of a dumbbell in the limit  $Re \gg 1$  is more complicated than envisaged by Harper & Chang (1968).

### 5. Fibre rotation with both sedimentation and shear

Herein, we examine the motion of a slender fibre sedimenting with velocity  $\mathbf{U}$  in an ambient simple shear flow. As referred to in the introduction, the first effects of inertia for both a sedimenting fibre and a neutrally buoyant fibre in simple shear flow are, in principle, calculable from a regular perturbation of the governing Navier–Stokes equations for small values of the appropriate Reynolds number –  $Re_{sed} = U l / \nu$  for sedimentation and  $Re = \dot{\gamma} l^2 / \nu$  for simple shear. Therefore, the inertial torque in either case is due to stresses associated with the  $O(Re_{sed})$  or  $O(Re)$  velocity field at distances from the fibre of order its own length. The latter are obtained from solving the inhomogeneous Stokes equations, valid in a region of  $O(l^3)$  around the fibre, the forcing term being the inertial acceleration,  $Re_{sed} D\mathbf{u}_0/Dt$  or  $Re D\mathbf{u}_0/Dt$ , arising from the leading-order Stokes velocity disturbance in either case; it is noted that  $D\mathbf{u}_0/Dt$  is not the same for the sedimentation and shear problems. However, that the Stokes velocity fields in sedimentation and shear are, respectively, even and odd functions of the displacement  $\mathbf{r}$  from the fibre centre, together with the linearity of the Stokes equations, implies that in the limit  $Re_{sed}, Re \ll 1$ , the leading-order inertial modifications of fibre motion under the combined effects of sedimentation and shear are given by superposition of the individual angular velocities.

When sedimenting in a quiescent fluid under the action of gravity, the velocity of a fibre depends rather weakly on its orientation even at  $Re_{sed} = 0$ , the maximum deviation from the direction of gravity being approximately  $19^\circ$ . Khayat & Cox (1989) determined the inertial torque on a fibre translating with a fixed velocity, and including the above orientation dependence of the actual settling velocity might therefore seem a hindrance to analysing the dynamics of fibre motion. However,  $\dot{\mathbf{p}}_{sed}$  has the same functional form in terms of either the orientation-dependent settling velocity  $\mathbf{U}$  or the (constant) gravitational force  $\mathbf{F}_g$ , and  $\mathbf{p}$ , in the limit of small  $Re_{sed}$ . This is seen from the fact that the inertial angular velocity in sedimentation being a pseudovector and a quadratic function of  $\mathbf{U}$  at leading order, must necessarily be of the form  $(k/\nu)(\mathbf{p} \cdot \mathbf{U})(\mathbf{p} \wedge \mathbf{U})$ ,  $k$  being constant in the limit  $Re_{sed} \ll 1$ . Using the expression

$$\mathbf{U} = \frac{d^2 \Delta \rho g (\ln \kappa)}{8\mu} [\mathbf{p}\mathbf{p} + \frac{1}{2}(\mathbf{I} - \mathbf{p}\mathbf{p})] \cdot \mathbf{1}_g, \tag{5.1}$$

for the Stokes settling velocity,† known from slender-body theory (see Cox 1970), one obtains

$$\boldsymbol{\Omega}_{sed} = k \frac{U^2}{2\nu} (\mathbf{p} \cdot \mathbf{1}_g)(\mathbf{p} \wedge \mathbf{1}_g), \tag{5.2}$$

for the angular velocity, where  $U = d^2 \Delta \rho g (\ln \kappa) / 8\mu$  serves as the velocity scale for sedimentation and may be used to define  $Re_{sed}$ . In turn, this yields the following

† The  $O(Re_{sed})$  inertial correction to this velocity will only affect the angular velocity at  $O(Re_{sed}^2)$ .

equation for the dimensional rate of change of fibre orientation:

$$\dot{\mathbf{p}}_{sed} = -\frac{5U^2}{16\nu \ln \kappa} (\mathbf{1}_g \cdot \mathbf{p})(\mathbf{I} - \mathbf{p}\mathbf{p}) \cdot \mathbf{1}_g. \quad (5.3)$$

Here, the numerical value of  $k$  has been used from Khayat & Cox's analysis (see Khayat & Cox 1989; also see the Appendix). In (5.3)  $\mathbf{1}_g$  denotes the unit vector in the direction of gravity, and  $\Delta\rho$  is the density difference driving sedimentation. Clearly, accounting for the orientation dependence of the fibre settling velocity presents no additional difficulty. We now proceed to investigate the three canonical instances where  $\mathbf{1}_g$  is directed along the flow, gradient and vorticity directions of simple shear. The case of gravity aligned with the vorticity arises in a vertically aligned cylindrical Couette cell. Gravity is aligned with the velocity gradient in a horizontal channel or a parallel plate rheometer with a vertical axis, while gravity is parallel to the flow direction in a vertical channel or pipe flow. With  $\mathbf{1}_g$  aligned along the vorticity axis, the inertial torque arising from sedimentation acts to move the fibre toward the plane of shear, now also the transverse plane of stability for the sedimentation problem. This enhances the orbital drift already present due to shear, the orbit phase  $\tau$ , and thence the value of  $Re_c$  remaining unchanged. Thus, while for  $Re < Re_c$  the fibre tends towards a tumbling motion in the plane of shear, for  $Re \geq Re_c$  the presence of a shear acts to select a unique stable orientation from the otherwise degenerate set in this transverse plane. This stable orientation makes an angle  $\phi_f$ , given by (3.30), with the flow direction. In the fibre-aligned coordinate system of §3.1, the dimensionless angular velocity on account of sedimentation is  $\dot{\theta}_{sed} = (\dot{p}_2)_{sed}/\dot{\gamma}$  with  $\mathbf{1}_g \equiv \mathbf{1}_z$  in (5.3), leading to the following modified equation for the change in orbit constant:

$$\frac{dC}{dt} = \left[ \frac{8\pi Re}{15 \ln \kappa} \sin^2 \theta \cos^2 \phi + \frac{5}{16} \frac{Re_{sed}^2}{Re \ln \kappa} \right] C. \quad (5.4)$$

The time  $t$  above is scaled with the shear rate. The ratio of the respective time scales of migration across a Jeffery orbit is given by

$$\frac{t_{sed}}{t_{shear}} \approx \frac{128\pi}{75} \sin^2 \theta \left( \frac{Re}{Re_{sed}} \right)^2. \quad (5.5)$$

Fibres translating perpendicular to a planar shear flow therefore exhibit the same qualitative orientation distribution as neutrally buoyant fibres at comparable  $Re$ .

The directions of the inertial torques due to sedimentation and shear are shown in figure 10 for  $\mathbf{1}_g$  along the flow and gradient directions. The torques depicted therein are for a nearly circular Jeffery orbit close to the plane of shear, and for orientations approximately aligned with the flow direction, the latter because the dominant inertial changes occur in the nearly aligned phases of a Jeffery orbit when the angular velocity of the fibre becomes small. Clearly, for  $\mathbf{1}_g$  in the flow direction, the sense of the inertial torques arising from the sedimentation and shear mechanisms is identical near the shearing plane. Thus, sufficiently large inertia will again lead to a fixed point  $\phi_f > 0$ , and the leading-order Jeffery torque then drives the stationary fibre towards the plane of shear. The fibre motion therefore remains qualitatively unaltered from that analysed in §3 so long as the either  $Re$  or  $Re_{sed}$  is large enough to allow for the existence of a stationary state. The details are, of course, different – for instance, the critical Reynolds number would now be a decreasing function of  $Re_{sed}$ . If  $Re$  and  $Re_{sed}$  are small enough to allow for fibre rotation, then sedimentation along the flow axis leaves the orbit constant  $C$  unchanged! This is because, as

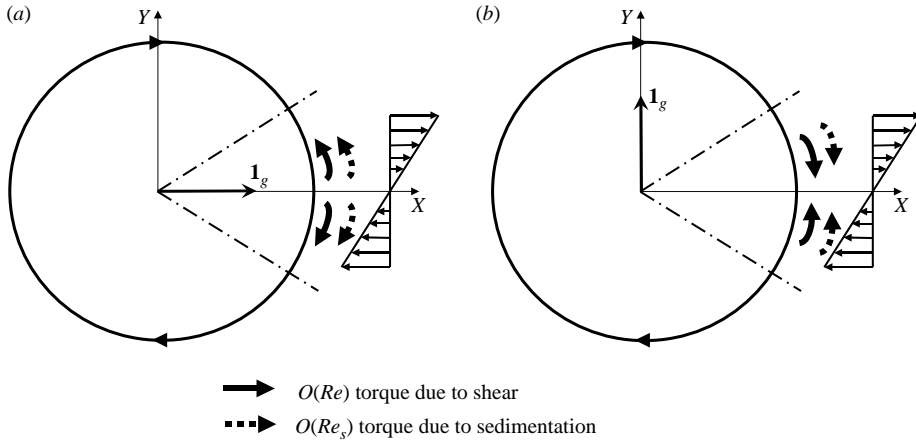


FIGURE 10. The sense of the inertial torques arising due to sedimentation and shear for tumbling motion in the plane of shear with  $\mathbf{1}_g$  along the flow (a) and gradient (b) directions.

noted earlier, the Jeffery orbits in the limit of infinite aspect ratio are meridians running between the points of intersection of the flow axis with the unit sphere. With  $\mathbf{1}_g = \mathbf{1}_x$ , the inertial drift due to sedimentation, being transversely isotropic about the flow axis, is along the same meridians and therefore consistent with a constant  $C$ . Thus, the drift in orbit constant remains identical to that in the presence of shear alone (see (3.23)) with only a quantitative change in the dynamics of the orbit phase.

We now look at the more interesting case of  $\mathbf{1}_g$  aligned in the gradient direction. With  $\mathbf{1}_g = \mathbf{1}_y$ , it may easily be shown using (3.20), (3.28) and (5.3) that the orbit equations are given by

$$\left. \begin{aligned} \dot{\theta} &= \sin \theta \cos \theta \sin \phi \cos \phi \left( 1 + \frac{28\pi Re}{15 \ln \kappa} \sin^2 \theta \sin \phi \cos \phi \right) - \frac{5}{16 \ln \kappa} \frac{Re_{sed}^2}{Re} \sin^2 \phi \sin \theta \cos \theta, \\ \dot{\phi} &= \frac{-1}{(\kappa_e^2 + 1)} (\kappa_e^2 \sin^2 \phi + \cos^2 \phi) - \frac{Re}{\ln \kappa} \sin^2 \theta \sin \phi \cos \phi \left( \frac{4\pi}{3} \sin \theta \sin^2 \phi - \frac{8\pi}{15} \sin \theta \cos^2 \phi \right) \\ &\quad - \frac{5}{16 \ln \kappa} \frac{Re_{sed}^2}{Re} \sin \phi \cos \phi, \end{aligned} \right\} \quad (5.6)$$

where  $\kappa_e = \beta\kappa$ , as before, is the equivalent aspect ratio of the fibre. The evolution of the orbit constant is governed by

$$\frac{dC}{dt} = \left( \frac{8\pi Re}{15 \ln \kappa} \sin^2 \theta \cos^2 \phi - \frac{5}{16 \ln \kappa} \frac{Re_{sed}^2}{Re} \right) C, \quad (5.7)$$

showing that for  $Re_{sed}$  however small, there always exists a finite section of the unit sphere around the vorticity axis, starting in which a fibre will eventually spiral towards the vorticity axis. In figure 11, with  $Re = 0.05$  and  $Re_{sed} = 0.04$ , a couple of fibre trajectories, in different regions of the unit sphere, exemplify this contrasting behaviour. One of them starts off closer to the flow–gradient plane and spirals out towards the flow–gradient plane, while the other, located very close to the vorticity direction, drifts in the opposite direction. Provided  $Re$  and  $Re_{sed}$  are small enough for the phase relationship to still be approximated by that along a Jeffery orbit, one

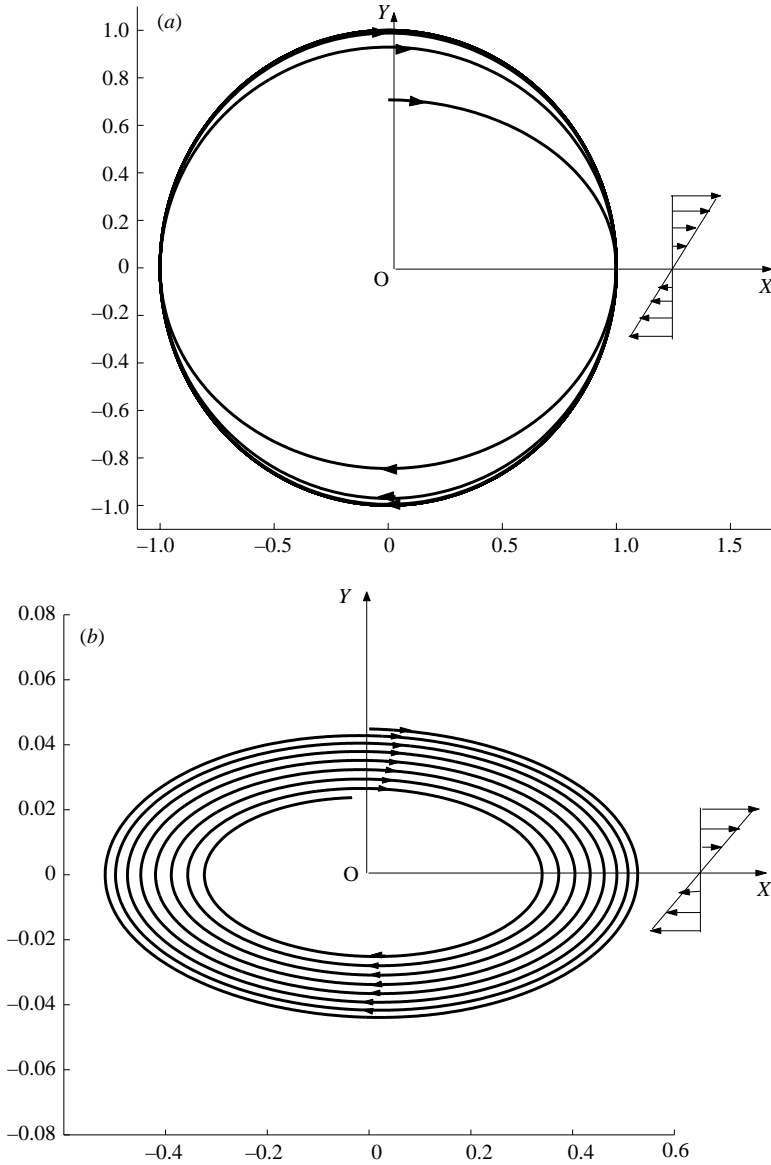


FIGURE 11. The opposite senses of the spiralling trajectories depending on the region of the unit sphere that they start from; here,  $Re = 0.05$ ,  $Re_{sed} = 0.04$  and  $\kappa = 20$ , and  $\mathbf{1}_g$  is along the gradient direction. In (a), the inertial torque due to shear is dominant, and the fibre spirals out towards the plane of shear, while in (b) for a point sufficiently close to the vorticity axis, the fibre drifts in the opposite direction due to the inertial torque arising from sedimentation.

may obtain an estimate of  $C$  for the orbit that separates the two basins of attraction corresponding to the plane of shear and the vorticity axis, respectively. Since the change of  $C$  over a  $2\pi$  cycle is  $o(1)$ , we have for the neutral orbit,

$$\int_0^{2\pi\kappa_e} \frac{8\pi Re}{15 \ln \kappa} \sin^2 \theta \cos^2 \phi dt \approx \frac{5\pi\kappa_e}{8 \ln \kappa} \frac{Re_{sed}^2}{Re}, \tag{5.8}$$



which may be rewritten as

$$\frac{8\pi Re C_n^2}{15} \int_0^{2\pi\kappa_e} \cot^2 \phi \cos^2 \theta dt = \frac{5\pi\kappa_e Re_{sed}^2}{8Re}, \tag{5.9}$$

the subscript ‘*n*’ corresponding to the neutral orbit. Since a fibre in a Jeffery orbit spends only an  $O(1/\kappa_e)$  fraction of a period away from orientations with  $\phi, \pi - \phi > O(1/\kappa_e)$ , the integral on the left-hand side may be approximated as  $2\pi\kappa_e^3 \cos^2 \theta_{\phi=0}$ . The value of  $\theta$  in the aligned phase may be related to the orbit constant by  $\theta_{\phi=0} = \cos^{-1}(1/\sqrt{1 + C_n^2 \kappa_e^2})$ , whence one finally obtains

$$C_n = \frac{1}{\beta\kappa \sqrt{\frac{128\pi Re^2}{75 Re_{sed}^2} - 1}}. \tag{5.10}$$

For  $Re_{sed}$  small, the fibre, for most initial orientations, still tends toward the plane of shear. With increasing  $Re_{sed}$  the phase relationship along an orbit changes and for  $Re_{sed}$  sufficiently large, a fixed point arises that is now of an opposite sign when compared to that found previously in presence of shear alone (see (3.30) in §3.1). This may be seen by considering the limiting form of the equation for  $\dot{\phi}$  in (5.6) for  $\phi$  small, and with  $\dot{\phi}$  set equal to zero. We have

$$0 = -\phi^2 - \frac{1}{\beta^2 \kappa^2} + \left[ \frac{8\pi Re}{15 \ln \kappa} \sin^2 \theta - \frac{5}{16 \ln \kappa} \frac{Re_{sed}^2}{Re} \right] \phi, \tag{5.11}$$

so the fixed point is given by

$$\begin{aligned} \phi'_f = & -\frac{1}{2} \left( \frac{5}{16 \ln \kappa} \frac{Re_{sed}^2}{Re} - \frac{8\pi Re}{15 \ln \kappa} \sin^2 \theta \right) \\ & + \frac{1}{2} \left[ \left( \frac{5}{16 \ln \kappa} \frac{Re_{sed}^2}{Re} - \frac{8\pi Re}{15 \ln \kappa} \sin^2 \theta \right)^2 - \frac{4}{\beta^2 \kappa^2} \right]^{1/2} \end{aligned} \tag{5.12}$$

which is negative provided

$$Re_{sed}^2 > \frac{128\pi}{75} Re^2 \sin^2 \theta. \tag{5.13}$$

Thus, one again has a non-rotating mode that now monotonically tends towards the vorticity axis. Unlike Leal’s observations for motion in a second-order fluid (see Leal 1975), however, the fibre will not start spiralling at any point en-route to the vorticity axis.

For instances where  $Re$  is sufficiently large for the fixed point  $\phi_f$  given by (3.30) to exist even when  $Re_{sed} = 0$ , an increase in  $Re_{sed}$  would lead to an intermediate regime where the two opposing inertial torques due to sedimentation and shear approximately balance each other, leading once again to a spiralling behaviour toward the plane of shear. Further increase in  $Re_{sed}$  leads to the stationary mode described above.

To summarize, the orientation behaviour of fibres settling in a shear flow depends on the direction of sedimentation relative to the plane of shear. With gravity directed along the flow and vorticity axes of a simple shear, settling fibres exhibit the same qualitative orientation behaviour as neutrally buoyant fibres. The behaviour of fibres settling in the gradient direction may, however, deviate significantly from quiescent settling depending on the relative values of  $Re$  and  $Re_{sed}$ . For sufficiently large

magnitude of the latter, the fixed point occurs with the fibre pointing upstream rather than downstream, i.e. with  $\phi_f$ , defined in §3, being negative; the resulting drift, in contrast to that seen for neutrally buoyant spheres, is towards the vorticity axis.

## 6. Conclusions

We have considered the first effects of fluid inertia on the rotational motion of an axisymmetric slender fibre in a simple shear flow when the Reynolds number based on the fibre length and velocity gradient is small. The inertially induced torque acting on the fibre can be related to a volume integral involving the Stokes flow velocity disturbance produced by the fibre by invoking the generalized reciprocal theorem. Because the dominant contribution to the volume integral comes at distances from the fibre axis comparable with the fibre length, the fluid velocity disturbance may be approximated as that due to a line of forces. This approach greatly simplifies the analysis. To validate the method and demonstrate its utility in another setting, we use the same method to reproduce Khayat & Cox's results for the torque on a sedimenting fibre in the Appendix.

At zero Reynolds number, a fibre in simple shear flow rotates in one of an infinite set of Jeffery orbits. In these orbits, the fibre axis circles around the vorticity axis of the base flow. Within most of the orbits the fibre axis comes very close to the flow direction and remains there for a large fraction of the time period. Fluid inertia alters this behaviour in two ways. First, it induces a small drift across orbits so that the fibre gradually spirals out toward the flow–gradient plane. Second, it changes the speed at which the fibre rotates through the orbit in such a way that the temporal period of the orbit lengthens with increasing Reynolds number, eventually diverging as  $O(Re_c - Re)^{-1}$ ,  $Re_c$  being the critical Reynolds number that scales with the inverse of the fibre aspect ratio. Above  $Re_c$ , the fibre ceases to rotate and remains close to the flow–vorticity plane, slowly migrating toward a fixed orientation near the flow direction.

Our analysis indicates the asymptotic behaviour of the fibre rotation for  $Re \ll 1$  and  $\kappa \gg 1$ . Only the leading-order Stokes flow velocity disturbance in the slender-body limit was retained, leading to relative errors of order  $1/\ln(\kappa)$ . However, previous experience suggests that the leading-order slender-body analysis gives a good quantitative estimate of the behaviour of fibres with aspect ratios larger than about 20. One way of judging the robustness of an asymptotic analysis is by comparison with experimental and/or numerical results. However, the experimental and numerical results on the rotation of prolate axisymmetric bodies in simple shear flow at finite  $Re$  are surprisingly sparse. Experimental observations of an aspect ratio 10 particle by Karnis *et al.* (1966) indicate that the particle migrates to an orbit in the flow–gradient plane in agreement with our analysis. However, the authors did not measure the rate of migration and no experiments were done above the critical Reynolds number at which we predict permanent flow alignment. The only numerical study of which we are aware is that of Qi & Luo (2003) who simulated the motion of a prolate spheroid with an aspect ratio of 2 for  $Re \geq 32$ . At moderate Reynolds numbers they found that the particles axis migrated toward the flow–gradient plane and subsequently rotated within this plane. This result suggests that the qualitative result of migration across Jeffery orbits toward the flow–gradient plane that is predicted for the limits  $\kappa \gg 1$  and  $Re \ll 1$  in this paper may be preserved over a wide range of particle Reynolds numbers and aspect ratios. Further experimental and numerical studies of the rotation of non-spherical particles would be valuable. In conducting the experimental studies one must

take care that secondary flows have a small influence on the fibre rotation. In the numerical studies, the boundary conditions far from the particle must be implemented carefully as the particle-induced fluid velocity disturbance may propagate to large distances from the fibre at larger  $Re$ .

While the analysis in this paper is restricted to  $Re \ll 1$ , the reciprocal theorem formulation in §2 is applicable for arbitrary  $Re$ . Extending the analysis to finite  $Re$  would require solving the linearized Navier–Stokes equations for the fluid velocity disturbance caused by the particle. As mentioned in the introduction, this analysis is considerably more involved than that for a settling particle at finite  $Re_{sed}$ . We plan to address this problem in a subsequent publication wherein we will also compare the theoretical analysis with numerical solutions of the full Navier–Stokes equations.

The orientation of fibres at non-zero Reynolds numbers plays a role in a number of applications including the orientation of pulp fibres during paper-making processes and the use of fibres for drag reduction. While these applications may involve higher Reynolds numbers, flexible fibres, and/or finite fibre concentrations, our results provide a good starting point for considering the effects of the fluid inertia associated with a mean shear flow on fibre orientation. The prediction that fibres remain aligned with the flow direction above a critical Reynolds number may play an important role in these applications. For example, it implies that rotary dispersion of fibre orientation caused by turbulence (Olson & Kerekes 1998) or particle interactions (Rahnama *et al.* 1993) would have to overcome a finite restoring torque in order to disperse the fibre axes away from the flow direction.

It has been widely observed that many types of fibre suspensions exhibit shear thinning and many mechanisms have been proposed that may account for the shear thinning in different circumstances, including fibre flexibility, fibre–fibre adhesion, and fibre alignment due to non-Newtonian solvent stresses. Since the stress caused by a fibre that is nearly aligned with the flow direction is much smaller than that produced by a rotating fibre, the present analysis suggests that dramatic shear thinning would arise in the vicinity of the critical Reynolds number for flow alignment. Since this phenomenon occurs at a modest particle Reynolds number, it may be accessible to rheological measurement.

This work was supported by NSF grant CTS-0332902.

## Appendix. Effect of inertia on the orientation of a sedimenting fibre

In what follows, we briefly outline the application of the generalized reciprocal theorem, introduced in §2, to a sedimenting fibre, first for small  $Re$  in §A.1, and later for  $O(1)$  values in §A.2; we compare our results to those previously obtained.

### A.1. Analysis for small but finite $Re_{sed}$

In a reference frame moving with the velocity  $\mathbf{U}$  of the translating fibre, the fluid velocity disturbance field  $\mathbf{u}'$  satisfies the steady Oseen equations in the limit  $\kappa \gg 1$ . Thus, the only inertial effect present is the convection of the velocity disturbance by the free-stream velocity  $-\mathbf{U}$ , and accordingly, we have  $\mathbf{f}'(\mathbf{r}) = -\mathbf{U} \cdot \nabla \mathbf{u}'$ ; here, as in (2.2),  $\mathbf{f}'$  represents the inertial terms in the Navier–Stokes equations. The generalized reciprocal theorem then takes the form

$$\int_S \mathbf{n} \cdot \boldsymbol{\sigma}' \cdot \tilde{\mathbf{u}} \, dS - Re_{sed} \int_V \mathbf{U} \cdot \nabla \mathbf{u}' \cdot \tilde{\mathbf{u}} \, dV = \int_S \mathbf{n} \cdot \tilde{\boldsymbol{\sigma}} \cdot \mathbf{u}' \, dS, \quad (\text{A } 1)$$

where  $Re_{sed} = Ul/\nu$  and  $V$  is the volume occupied by the fluid.

The fields  $(\tilde{\mathbf{u}}, \tilde{\boldsymbol{\sigma}})$  are again chosen to correspond to the Stokes problem of a fibre rotating with angular velocity  $\tilde{\boldsymbol{\Omega}}$  in a quiescent fluid. The subsequent manipulations remain identical to those detailed in §2, and one obtains

$$\mathcal{L}_{sed} \cdot \tilde{\boldsymbol{\Omega}} = Re_{sed} \int_V \mathbf{U} \cdot \nabla \mathbf{u}' \cdot \tilde{\mathbf{u}} \, d\mathbf{r} \quad (\text{A } 2)$$

for the torque on the translating fibre with  $\tilde{\mathbf{u}}$  given by (2.3). All variables in (A 2) have been made dimensionless using the velocity scale  $U$  and the length  $l$  of the fibre. It is now shown that the dominant contribution to the volume integral in (A 2) comes from  $r \sim O(1)$ , that is, a region around the fibre whose linear dimension scales as the fibre length, so that the leading-order inertial correction to the fibre torque is  $O(Re_{sed})$ . Considering a cylindrical region  $\bar{r} \sim O(\kappa^{-1})$  around the fibre axis, we observe that  $\tilde{\mathbf{u}}, \mathbf{u}' \sim \ln \bar{r}$ ,  $\nabla \mathbf{u}' \sim 1/\bar{r}$  and  $dV \sim \bar{r} \, d\bar{r}$ . Thus, the near-field contribution to the volume integral scales as  $\ln \bar{r} \, d\bar{r}$  for  $\bar{r} \sim O(\kappa^{-1})$ , being asymptotically small for large  $\kappa$ . Again, for distances greater than the inertial screening length, i.e.  $r > Re_{sed}^{-1}$ ,  $\mathbf{u}'$  decays at least as fast as  $1/r$ , while  $\tilde{\mathbf{u}}$ , being of a dipole character, is  $O(1/r^2)$ . The integrand then becomes  $O(1/r^4)$ , ensuring that the contribution from the outer region is  $O(Re_{sed})$  smaller when compared to that from  $r \sim O(1)$ .

The analysis for the first effects of inertia may therefore be carried out in Fourier space, treating the fibre as a line distribution of forces, and using the Stokes expression for the velocity disturbance  $\mathbf{u}'$ . The expression for the Fourier transform of the latter is given by

$$\hat{\mathbf{u}}'(\mathbf{k}) = \frac{1}{(\ln \kappa)} \hat{\mathbf{G}}_0(\mathbf{k}) \cdot [\mathbf{U} \cdot (\mathbf{I} - \frac{1}{2} \mathbf{p} \mathbf{p})] \frac{\sin\{2\pi(\mathbf{k} \cdot \mathbf{p})\}}{2\pi(\mathbf{k} \cdot \mathbf{p})}, \quad (\text{A } 3)$$

where the definition of the Fourier transform is the same as that used previously in the text, namely that given by equations (3.1) and (3.2). One obtains for the torque,

$$\begin{aligned} \mathcal{L}_{sed} \cdot \tilde{\boldsymbol{\Omega}} &= Re_{sed} \int_V (\mathbf{U} \cdot \nabla \mathbf{u}') \cdot \tilde{\mathbf{u}} \, d\mathbf{r} \\ &= Re_{sed} \int -2\pi i \mathbf{k} \cdot \mathbf{U} \hat{\mathbf{u}}'(-\mathbf{k}) \cdot \hat{\tilde{\mathbf{u}}}(\mathbf{k}) \, d\mathbf{k}. \end{aligned} \quad (\text{A } 4)$$

Since  $\tilde{\boldsymbol{\Omega}}$  is arbitrary, we have

$$\mathcal{L}_{sed} = -\frac{4 Re_{sed}}{\pi^2 (\ln \kappa)^2} \mathbf{U} \cdot (\mathbf{I} - \frac{1}{2} \mathbf{p} \mathbf{p}) \mathbf{U} : \left[ \int \frac{\mathbf{k}}{(\mathbf{k} \cdot \mathbf{p})} \left( \frac{\mathbf{I}}{k^4} - \frac{\mathbf{k} \mathbf{k}}{k^6} \right) \sin(2\pi \mathbf{k} \cdot \mathbf{p}) j_1(2\pi \mathbf{k} \cdot \mathbf{p}) \, d\mathbf{k} \right] \wedge \mathbf{p}, \quad (\text{A } 5)$$

where we have used the expression for  $\hat{\tilde{\mathbf{u}}}(\mathbf{k})$  from §2, and (3.7) for  $\hat{\mathbf{G}}_0(\mathbf{k})$ . In a fibre-aligned coordinate system with the 1- and 2-directions in the plane of settling (spanned by  $\mathbf{p}$  and  $\mathbf{U}$ ), the former being along the fibre axis  $\mathbf{p}$ , the only non-zero component of the torque is perpendicular to this plane; thus, (A 5) reduces to

$$(\mathcal{L}_{sed})_3 = -\frac{2 Re_{sed}}{\pi^2} \frac{\sin 2\theta}{(\ln \kappa)^2} \int \frac{(k_1^2 + k_3^2 - k_2^2/2)}{k^6} \sin(2\pi k_1) j_1(2\pi k_1) \, d\mathbf{k}, \quad (\text{A } 6)$$

where  $\theta$  is the angle between  $\mathbf{U}$  and  $\mathbf{p}$ . Using polar coordinates in the  $(k_2, k_3)$ -plane, the integral in (A 6) can be expressed in terms of standard integrals involving the spherical Bessel function  $j_1$ , readily available, for instance, in Gradshteyn & Ryzhik (1965). The Fourier integral is thus found to be  $5\pi^3/12$ , whence the dimensional

inertial torque is given by

$$(\mathcal{L}_{sed})_3 = -\frac{5\pi}{6(\ln \kappa)^2} \sin 2\theta Re_{sed}(\mu Ul^2). \tag{A 7}$$

This is verified as being identical to the result obtained by Khayat & Cox (1989) in the limit  $Re_{sed} \ll 1$  – see equation (6.22) in their paper.

A.2. Finite- $Re_{sed}$  analysis

For  $O(1)$  values of  $Re_{sed}$ , the expression for the inertial torque in terms of the volume integral in (A 2) is still valid. The velocity disturbance  $\mathbf{u}'$  now corresponds to finite  $Re_{sed}$  and is obtained by solving the linearized Navier–Stokes equations. In the small- $Re_{sed}$  analysis above, the fibre forcing per unit length was taken to be the same as its inertialess value, this being consistent with the order of terms retained therein. For the finite- $Re_{sed}$  case, the force per unit length of the translating fibre is, in principle, an unknown, and must be treated as such when solving the equations of motion. Provided the Reynolds number based on the fibre diameter,  $Re_{d_{sed}} = Ud/\nu$ , is small, however, one may continue to use the Stokes value for the fibre forcing. In order to see this, we first note that the drag per unit length on a fibre in the limit  $Re_{sed} \gg 1$ , i.e. with the inertial screening length ( $\nu/U$ ) being much smaller  $l$ , is  $O(1/\ln(Re_{d_{sed}}^{-1}))$ . This result may, of course, be obtained from analysing the two-dimensional problem of an infinite cylinder translating at small but finite  $Re_{d_{sed}}$  (for instance, see Proudman & Pearson 1957). Since  $Re_{d_{sed}} = Re_{sed}/\kappa$ , the drag per unit length in the limit  $Re_{sed} \gg 1$  may be expanded as

$$\lim_{Re_{sed} \gg 1} f_{fibre} = O\left(\frac{1}{\ln \kappa}\right) + O\left(\frac{\ln Re_{sed}}{(\ln \kappa)^2}\right), \tag{A 8}$$

where the leading term is the value of forcing for  $Re_{sed} = 0$ . It is then evident that so long as  $Re_{sed} \ll \kappa$  (or  $Re_{d_{sed}} \ll 1$ ), it suffices to use the fibre forcing in the inertialess limit even for finite  $Re_{sed}$ . Thus, the Stokes value for the fibre forcing remains a good approximation as long as the region around it, of extent its own diameter, remains viscous dominated. This fact allowed us, in the earlier section, to estimate the contribution from the inner region of (dimensionless) extent  $O(\kappa^{-1})$  around the fibre to be asymptotically small, being of  $O(\ln \kappa/\kappa)$ . This estimate, though independent of  $Re_{sed}$ , is valid provided  $Re_{d_{sed}} \ll 1$ , and allows the analysis to again be performed in Fourier space for large  $\kappa$ .

The torque is still given by the Fourier integral in (A 4), with the Fourier transform  $\hat{\mathbf{u}}'(\mathbf{k})$  of the fibre velocity disturbance:

$$\hat{\mathbf{u}}'(\mathbf{k}) = \frac{8\pi}{(\ln \kappa)} \frac{[\mathbf{U} \cdot (\mathbf{I} - \frac{1}{2}\mathbf{p}\mathbf{p})] \cdot (\mathbf{I} - \mathbf{k}\mathbf{k}/k^2) \sin\{2\pi(\mathbf{k} \cdot \mathbf{p})\}}{[Re_{sed}2\pi i \mathbf{k} \cdot \mathbf{U} + (2\pi k)^2] 2\pi(\mathbf{k} \cdot \mathbf{p})}, \tag{A 9}$$

obtained from Fourier transforming the Oseen equation. Using (A 9), we obtain the finite- $Re_{sed}$  analogue of (A 5):

$$\begin{aligned} \mathcal{L}_{sed} = & -\frac{16 Re_{sed}}{(\ln \kappa)^2} \mathbf{U} \\ & \cdot (\mathbf{I} - \frac{1}{2}\mathbf{p}\mathbf{p}) \mathbf{U} : \left[ \int \frac{\mathbf{k}(\mathbf{I}/k^2 - \mathbf{k}\mathbf{k}/k^4)}{(\mathbf{k} \cdot \mathbf{p})[Re_{sed}2\pi i \mathbf{k} \cdot \mathbf{U} + (2\pi k)^2]} \sin(2\pi \mathbf{k} \cdot \mathbf{p}) j_1(2\pi \mathbf{k} \cdot \mathbf{p}) d\mathbf{k} \right] \wedge \mathbf{p}. \end{aligned} \tag{A 10}$$

In order to evaluate the integral in (A 10), we use the following relations for the spherical Bessel functions:

$$j_0(2\pi\mathbf{k} \cdot \mathbf{p}) = \frac{\sin(2\pi\mathbf{k} \cdot \mathbf{p})}{2\pi\mathbf{k} \cdot \mathbf{p}} = \frac{1}{2} \int_{-1}^1 e^{-i2\pi(\mathbf{k} \cdot \mathbf{p})s} ds, \quad (\text{A } 11)$$

$$j_1(2\pi\mathbf{k} \cdot \mathbf{p}) = \frac{i}{2} \int_{-1}^1 e^{-i2\pi(\mathbf{k} \cdot \mathbf{p})s} s ds. \quad (\text{A } 12)$$

Substituting, the Fourier integral becomes

$$\begin{aligned} & -\frac{16 Re_{sed}}{(\ln \kappa)^2} [\mathbf{U} \cdot (\mathbf{I} - \frac{1}{2} \mathbf{p} \mathbf{p})] \cdot \left[ \frac{i}{4} \int_{-1}^1 \int_{-1}^1 ds ds' s' \right. \\ & \left. \times \int \frac{(\mathbf{k} \cdot \mathbf{U})(\mathbf{I}/k^2 - \mathbf{k}\mathbf{k}/k^4)}{[Re_{sed} 2\pi i \mathbf{k} \cdot \mathbf{U} + (2\pi k)^2]} e^{-i2\pi \mathbf{k} \cdot \mathbf{p}(s+s')} d\mathbf{k} \right] \wedge \mathbf{p}, \end{aligned}$$

which may be rewritten as

$$\begin{aligned} & \frac{2 Re_{sed}}{\pi(\ln \kappa)^2} [\mathbf{U} \cdot (\mathbf{I} - \frac{1}{2} \mathbf{p} \mathbf{p})] \cdot \left\{ \int_{-1}^1 \int_{-1}^1 ds ds' s' \mathbf{U} \cdot \frac{\partial}{\partial \mathbf{r}} \left[ \mathbf{I} \int d\mathbf{k} \frac{e^{-i2\pi \mathbf{k} \cdot \mathbf{a}}}{k^2 [Re_{sed} 2\pi i \mathbf{k} \cdot \mathbf{U} + (2\pi k)^2]} \right. \right. \\ & \left. \left. + \frac{1}{4\pi^2} \frac{\partial^2}{\partial \mathbf{r} \partial \mathbf{r}} \int d\mathbf{k} \frac{e^{-i2\pi \mathbf{k} \cdot \mathbf{a}}}{k^4 [Re_{sed} 2\pi i \mathbf{k} \cdot \mathbf{U} + (2\pi k)^2]} \right] \right\} \wedge \mathbf{p}, \quad (\text{A } 13) \end{aligned}$$

where the vector  $\mathbf{a} = \mathbf{p}(s + s')$ . It may be shown that the non-trivial integrands in (A 13) are only functions of  $w = s + s'$ . It is convenient to choose a coordinate system with  $\mathbf{U} = U\mathbf{1}_1$ , whence  $\mathbf{p} = (\sin \theta \mathbf{1}_2 - \cos \theta \mathbf{1}_1)$ ,  $\theta$  again being the angle between  $\mathbf{U}$  and  $\mathbf{p}$ . Thus,  $k_1$  is the Fourier coordinate along, and  $(k_2, k_3)$  the coordinates transverse to the direction of translation. Integration with respect to  $k_1$  can be formulated as a contour integral. The denominators of the two integrands are fourth-order and sixth-order polynomials in  $k_1$ , respectively. The former may be shown to have four roots along the imaginary axis in the complex  $k_1$ -plane, while the latter has the same four roots, two of them being repeated ones; the roots in either case are only functions of  $k_t = (k_2^2 + k_3^2)^{1/2}$ . Application of the method of residues then leads to an expression in terms of exponentials of  $k_t w$ . On changing to polar coordinates in the transverse plane, namely  $k_2 = k_t \cos \phi$ ,  $k_3 = k_t \sin \phi$ , the integration over  $\phi$  can be carried out simply, yielding cylindrical Bessel functions of  $k_t w$  of the zeroth order. The resulting integrals are then of a standard form and may be shown to yield the expression for the torque found by Khayat & Cox in equation (6.6) of their paper. The torque in the final form is given by

$$\begin{aligned} \frac{\mathcal{L}_{sed}}{\mu U l^2} &= -\frac{2\pi \sin \theta}{(\ln \kappa)^2} \left[ \frac{\cos \theta}{Re_{sed}(1 - \cos \theta)} \left\{ 2 + 2 \frac{\exp(-Re_{sed}(1 - \cos \theta)) - 1}{Re_{sed}(1 - \cos \theta)} \right. \right. \\ & \left. \left. - E_1[Re_{sed}(1 - \cos \theta)] - \ln[Re_{sed}(1 - \cos \theta)] - \gamma \right\} + \frac{\cos \theta}{Re_{sed}(1 + \cos \theta)} \right. \\ & \left. \times \left\{ 2 + 2 \frac{\exp(-Re_{sed}(1 + \cos \theta)) - 1}{Re_{sed}(1 + \cos \theta)} - E_1[Re_{sed}(1 + \cos \theta)] \right\} \right] \end{aligned}$$

$$\begin{aligned}
& -\ln[Re_{sed}(1 + \cos \theta)] - \gamma \} - 2 \left\{ \frac{1}{Re_{sed}(1 - \cos \theta)} \right. \\
& \times \left( 1 - \frac{1 - \exp(-Re_{sed}(1 - \cos \theta))}{Re_{sed}(1 - \cos \theta)} \right) - \frac{1}{Re_{sed}(1 + \cos \theta)} \\
& \left. \times \left( 1 - \frac{1 - \exp(-Re_{sed}(1 + \cos \theta))}{Re_{sed}(1 + \cos \theta)} \right) \right\} \Bigg], \quad (A 14)
\end{aligned}$$

where  $\gamma$  is Euler's constant and

$$E_1(z) = \int_z^\infty \frac{e^{-\tau}}{\tau} d\tau.$$

#### REFERENCES

- AIDUN, C. K., LU, Y. & DING, E. J. 1998 Direct analysis of particulate suspensions with inertia using the discrete Boltzmann equation. *J. Fluid Mech.* **373**, 287.
- ANCZUROWSKI, E. & MASON, S. G. 1967 Kinetics of flowing dispersions. 3. Equilibrium orientations of rods and discs (experimental) *J. Colloid Interface Sci.* **23**(4), 533.
- BARTRAM, E., GOLDSMITH, H. L. & MASON, S. G. 1975 Particle motions in non-Newtonian media.3. Further observations in elastoviscous fluids. *Rheol. Acta* **14**, 776.
- BATCHELOR, G. K. 1970 Slender-body theory for particles of arbitrary cross-section in Stokes flow. *J. Fluid Mech.* **44**, 419.
- BREHERTON, F. P. 1964 The motion of rigid particles in a shear flow at low Reynolds number. *J. Fluid Mech.* **14**, 284.
- COX, R. G. 1970 The motion of long slender bodies in a viscous fluid. Part 1. General theory. *J. Fluid Mech.* **44**, 791.
- COX, R. G. 1971 The motion of long slender bodies in a viscous fluid. Part 2. Shear flow. *J. Fluid Mech.* **45**, 625.
- DING, E. J. & AIDUN, C. K. 2000 The dynamics and scaling law for particles suspended in shear flow with inertia. *J. Fluid Mech.* **423**, 317.
- FENG, J., HU, H. H. & JOSEPH, D. D. 1994 Direct simulation of initial value problems for the motion of solid bodies in a Newtonian fluid Part 1. Sedimentation. *J. Fluid Mech.* **261**, 95.
- GRADSHTEYN, I. S. & RYZHIK, I. M. 1965 *Table of Integrals, Series and Products*. Academic.
- HAPPEL, J. & BRENNER, H. 1973 *Low Reynolds Number Hydrodynamics*. Noordhoff.
- HARPER, E. Y. & CHANG, I-DEE 1968 Maximum dissipation resulting from lift in a slow viscous shear flow. *J. Fluid Mech.* **33**, 209–225.
- JEFFERY, G. B 1922 The motion of ellipsoidal particles immersed in a viscous fluid. *Proc. R. Soc. Lond. A* **102**, 161.
- KARNIS, A., GOLDSMITH, H. L. & MASON, S. G. 1966 The flow of suspensions through tubes.V. Inertial effects. *Can. J. Chem. Engng* **44**, 181.
- KHAYAT, R. E. & COX, R. G. 1989 Inertia effects on the motion of long slender bodies. *J. Fluid Mech.* **209**, 435.
- LEAL, L. G. 1975 The slow motion of slender rod-like particles in a second order fluid. *J. Fluid Mech.* **69**, 305.
- LEAL, L. G. & HINCH, E. J. 1971 Effect of weak Brownian rotations on particles in shear flow. *J. Fluid Mech.* **46**, 685.
- LOVALENTI, P. M. & BRADY, J. F. 1993 The hydrodynamic force on a rigid particle undergoing arbitrary time-dependent motion at small Reynolds number. *J. Fluid Mech.* **256**, 561.
- MCLAUGHLIN, J. B. 1991 Inertial migration of a small sphere in linear shear flows. *J. Fluid Mech.* **224**, 261.
- OLSON, J. A. & KERÉKES, R. J. 1998 The motion of fibres in turbulent flow *J. Fluid Mech.* **377**, 47.

- PROUDMAN, I. & PEARSON, J. R. A. 1957 Expansions at small Reynolds numbers for the flow past a sphere and a circular cylinder. *J. Fluid Mech.* **2**, 237.
- QI, D. & LUOI, L. 2003 Transitions in rotations of a nonspherical particle in a three-dimensional moderate Reynolds number Couette flow. *Phys. Fluids* **14**, 4440.
- RAHNAMA, M., KOCH, D. L., ISO, Y. & COHEN, C. 1993 Hydrodynamic translational diffusion in fibre suspensions subject to simple shear flow. *Phys. Fluids* **5**, 849.
- SAFFMAN, P. G. 1956 On the motion of small spheroidal particles in a viscous liquid. *J. Fluid Mech.* **1**, 540.
- SAFFMAN, P. G. 1965 The lift on a small sphere in slow shear flow. *J. Fluid Mech.* **22**, 385.
- STONE, H. A., BRADY, J. F. & LOVALENTI, P. M. 2005 Inertial effects on the rheology of suspensions and on the motion of individual particles. *J. Fluid Mech.* in press.